Advancing chloroplast synthetic biology through high-throughput plastome engineering of *Chlamydomonas reinhardtii*

René Inckemann[1,2†*], Tanguy Chotel[1,2†], Cedric K. Brinkmann[1], Michael Burgis[1], Laura Andreas[1], Jessica Baumann[1], Priyati Sharma, Melanie Klose[1], James Barret[5], Fabian Ries[4], Nicole Paczia[1], Timo Glatter[1], Felix Willmund[3,4], Luke C. M. Mackinder[5] and Tobias J. Erb[1,2*]

[†] These authors contributed equally to this work.

* Corresponding authors

[1] Department of Biochemistry & Synthetic Metabolism, Max Planck Institute for Terrestrial Microbiology, Marburg, Germany

[2] SYNMIKRO Center of Synthetic Microbiology, Marburg, Germany

[3] Department of Biology, University of Marburg, Marburg, Germany

[4] Group Genetics of Eukaryotes, TU Kaiserslautern, Kaiserslautern, Germany

[5] Centre for Novel Agricultural Products (CNAP), Department of Biology, University of York

Abstract

Chloroplast synthetic biology holds promise for developing improved crops through improving the function of plastids. However, chloroplast engineering efforts face limitations due to the scarcity of genetic tools and the low throughput of plant-based systems. To address these challenges, we here established *Chlamydomonas reinhardtii* as a prototyping chassis for chloroplast synthetic biology. We developed an automation workflow that enables the generation, handling, and analysis of thousands of transplastomic strains in parallel, expanded the repertoire of selection markers for chloroplast transformation, established new reporter genes, and characterized over 140 regulatory parts, including native and synthetic promoters, UTRs, and intercistronic expression elements. We integrated the system within the Phytobrick cloning standard and demonstrate several applications, including a library-based approach to develop synthetic promoter designs in plastids. Finally, we provide a proof-of-concept for prototyping novel traits in plastids by introducing a chloroplast-based synthetic photorespiration pathway and demonstrating a twofold increase in biomass production. Overall, our study advances chloroplast engineering, and provides a promising platform to rapidly prototype chloroplast manipulations before their transfer into higher plants and crops.

Main

Synthetic biology offers promising prospects for developing photosynthetic organisms and crop varieties with improved traits.[1] These include enhanced resilience to extreme weather conditions, such as heat waves and drought[2], superior nutrient content, like omega fatty acids[3] and vitamins[4], and improved yield, for instance through more efficient photorespiratory bypasses[5–10] or entirely new-to-nature carbon fixation cycles.[11–15] However, realizing the full potential of synthetic biology in photosynthetic eukaryotes will require significant advancements in genetic engineering capabilities that go beyond traditional breeding and gene-editing techniques.[16]

In particular chloroplasts have become an increasing target for advanced engineering efforts.[7,17–19] These organelles harbor the photosynthetic apparatus and house several metabolic processes of high interest for the engineering of novel traits. For example chloroplast genome (plastome)-based engineering of plastid isoprenoid metabolism has recently proven a highly effective strategy for the production of high-value compounds, such as astaxanthin or artemisinin.[20,21] Moreover, several subunits of the light-harvesting and carbon fixation machineries are encoded by the plastome, which makes the direct manipulation of the chloroplast genome central for any efforts that aim at improving photosynthetic yield. One current example are efforts of integrating carboxysome and pyrenoid bases CO2-concentrating mechanism into plant chloroplasts to boost photosynthetic efficiency[22–30]

These examples emphasize the growing need to develop advanced genetic tools for the direct manipulation of the plastome. However, chloroplast genome engineering offers additional advantages compared to nuclear genome-based engineering strategies of chloroplast functions. Expression of transgenes from the chloroplast genome benefits from precise genomic integration, the absence of (nuclear) silencing mechanisms, significant higher protein levels that can be achieved, and improved genetic containment, as transgenes are not transmitted by pollen due to the strict maternal inheritance of chloroplasts.[31]

Yet, despite all these advantages, genetic engineering of the plastid is still constrained to only a handful of available genetic elements and tools.[32,33] Currently, only one or two selection markers are used on a routine base.[34] Moreover, only a small number of natural gene expression elements (5’UTR, 3’UTR, promoters) are available, which limits the number of genes that can be stacked, and provides little control over their expression strength.[32] This limited tool set is even more constrained, as gene expression elements cannot be simply re-used because of the high homologous recombination frequency of the plastome, which is observed for sequences as short as 50 base pairs.[35]

68 Thus, to bring the applications of synthetic biology in plastids to the level of versatility and
69 complexity that is available for other organisms, methods for the systematic assembly and
70 large-scale characterization of gene expression elements in chloroplasts are urgently
71 required.[19,36,37] However, the long generation times of photosynthetic eukaryotes, and the
72 absence of suitable model systems that are compatible with high-throughput handling routines
73 have impeded the development of genetic tools for the chloroplast, thus far.[38] Consequently,
74 the systematic development of plastid transgene expression strategies and the prototyping of
75 complex genetic designs in chloroplasts have remained beyond reach.

76 In this study, we aimed at overcoming above shortcomings, by establishing *Chlamydomonas*
77 *reinhardtii* as chassis for advancing chloroplast synthetic biology. This fast-growing, uni-
78 cellular green algae contains a single chloroplast and can be cultivated in high-throughput
79 formats[39–42], which makes it a highly suitable model for plastome-engineering. To generate,
80 handle and analyze thousands of transplastomic *C. reinhardtii* strains in parallel, we
81 developed an automation workflow, expanded the number of selection markers for chloroplast
82 transformation, and established several new reporter genes for fluorescence and
83 luminescence-based readouts and cell sorting.

84 Building on these resources, we systematically characterized a collection of more than 140
85 regulatory parts, including 35 different 5'UTRs, 36 3'UTRs, 59 promoters, and 16 intercistronic
86 expression elements (IEEs) for advanced gene stacking. We embedded these genetic parts
87 within a Phytobrick/Modular cloning (MoClo) framework[19] for the standardized and automated
88 assembly of genetic constructs that are compatible with existing *C. reinhardtii*, and plant
89 MoClo resources. Using this MoClo routine allowed us to rapidly assemble and characterize
90 gene element combinations at multiple insertion loci to establish multi-transgene constructs
91 that range across more than three orders of magnitude in expression strength. Finally, we
92 showcase the utility of our tools by developing more than 30 synthetic promoters through a
93 pooled library-based approach in chloroplasts and provide another real-world application case
94 by introducing a recently reported synthetic photorespiration pathway into the chloroplast[7] .

95 Overall, our work provides a high-throughput workflow for chloroplast synthetic biology and a
96 foundational set of genetic elements for the convenient engineering of the chloroplast that is
97 freely available to the community. Because of a high transferability of results between the
98 chloroplasts of *C. reinhardtii* and the chloroplasts of other organisms[43–45], our platform opens
99 the possibility for rapid prototyping of new traits before transfer into higher plants and crops.

Results

Automation workflow for high-throughput characterization of transplastomic *C. reinhardtii* strains

To facilitate the systematic characterization of genetic parts across thousands of transplastomic *C. reinhardtii* strains, we developed an automated chloroplast engineering workflow. This workflow is based on solid-media cultivation and leverages a contactless liquid-handling robot to enhance our capacity for handling an increased number of strains (Fig. 1). In brief, the workflow relies on the automated picking of transformants into a standardized 384 format and subsequent restreaks to achieve homoplasy, using a Rotor screening robot. These colonies are then organized into a 96-array format for high-throughput biomass growth, liquid-medium transfer and/or additional screens such as reporter gene analysis. The later involves using the Rotor screening robot for the transfer of biomass from 96-array agar plates into multi-well plates filled with water. Following resuspension, the optical density is measured at 750 nm (OD750), and a contact-free liquid handler is used for cell number normalization, medium transfer, and the supplementation of additional compounds (e.g., the NanoLuc substrate). Transitioning to a (partially) solid-media based workflow proved to be an advancement over previous techniques that solely relied on liquid-medium cultures, which inherently limited the number of strains that can be handled in parallel. Overall, this automation workflow was essential for generating and managing the 3,156 individual transplastomic strains that were used in this study, as presented in the following.

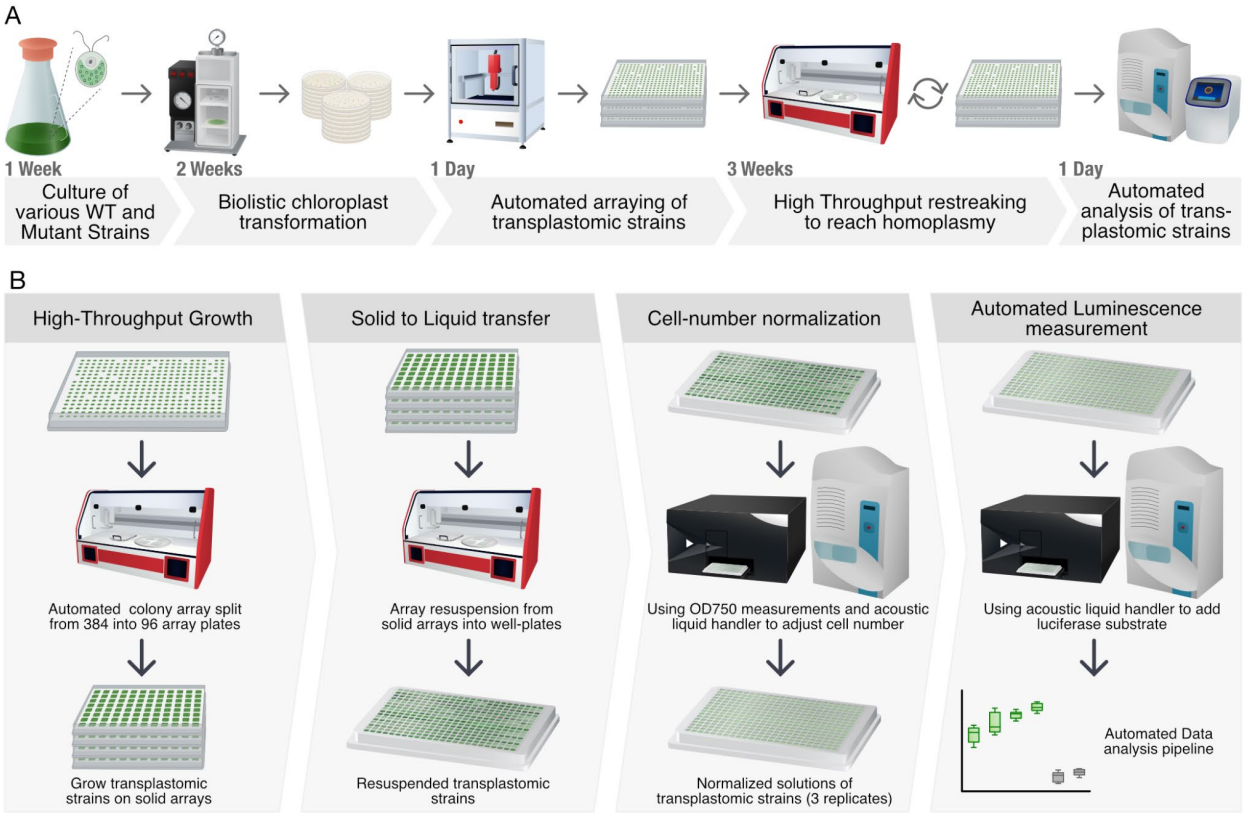

Figure 1: Workflow for generation and high-throughput characterization of transplastomic *C. reinhardtii* strains

a, Automated transplastomic strain generation workflow. Chloroplast transformation is performed via biolistic transformation via particle gun, subsequent automated arraying of transformants via PixL picking robot. Transplastomic strains are restreaked three times to reach homoplasmy via Rotor screening robot. Automated genotyping of transplastomic strains is performed via acoustic liquid handler and qPCR analysis to confirm homoplasmy. **b** High throughput characterization of transplastomic strains. Colonies are transferred to 96-well formats for biomass cultivation, preparing for reporter gene measurement. Rotor robot is then used to transfer biomass from agar (96 strains/plate) to multiwell plates for resuspension. Optical density at 750 nm (OD_{750}) is measured, and the Echo liquid handler is used for cell normalization and NanoLuc luciferase substrate addition.

Establishing a foundational set of genetic parts for chloroplast engineering

We next established a foundational set of >300 genetic parts for plastome manipulation of *C. reinhardtii* , which we embedded in a standardized MoClo framework[46,47] (Fig. 2a, Extended Data Fig. 1). This set of parts encompasses regulatory elements, such as 5'UTRs, 3'UTRs, Intercistronic expression elements (IEEs), derived from the chloroplast genome of *C. reinhardtii*, tobacco and even includes some synthetic regulatory elements. Additionally, it also contains parts for integration into various sites within the chloroplast genome (Extended Data Fig. 1). Our repository also encompasses several selection markers and reporter genes, which we identified and validated for *C. reinhardtii*. Beyond the well-established spectinomycin selection marker, we introduced tobramycin as a selection system for chloroplast transformation in *C. reinhardtii* (Fig. 2b, Extended Data Fig 2.c). This selection marker exhibited transformations efficiencies that are comparable to spectinomycin-based plastome

144 selection, with 100-1,000 colonies per plate and ~10µg DNA biolistic transformation. We also
145 integrated and validated kanamycin[48] and phosphite[49,50] selection markers in our parts library,
146 as well as an arginine-based selection system[51] that complements arginine auxotrophy in a
147 *C. reinhardtii* Arg9 deletion background (Fig. 2b, Extended Data Fig. 2d).

148

149

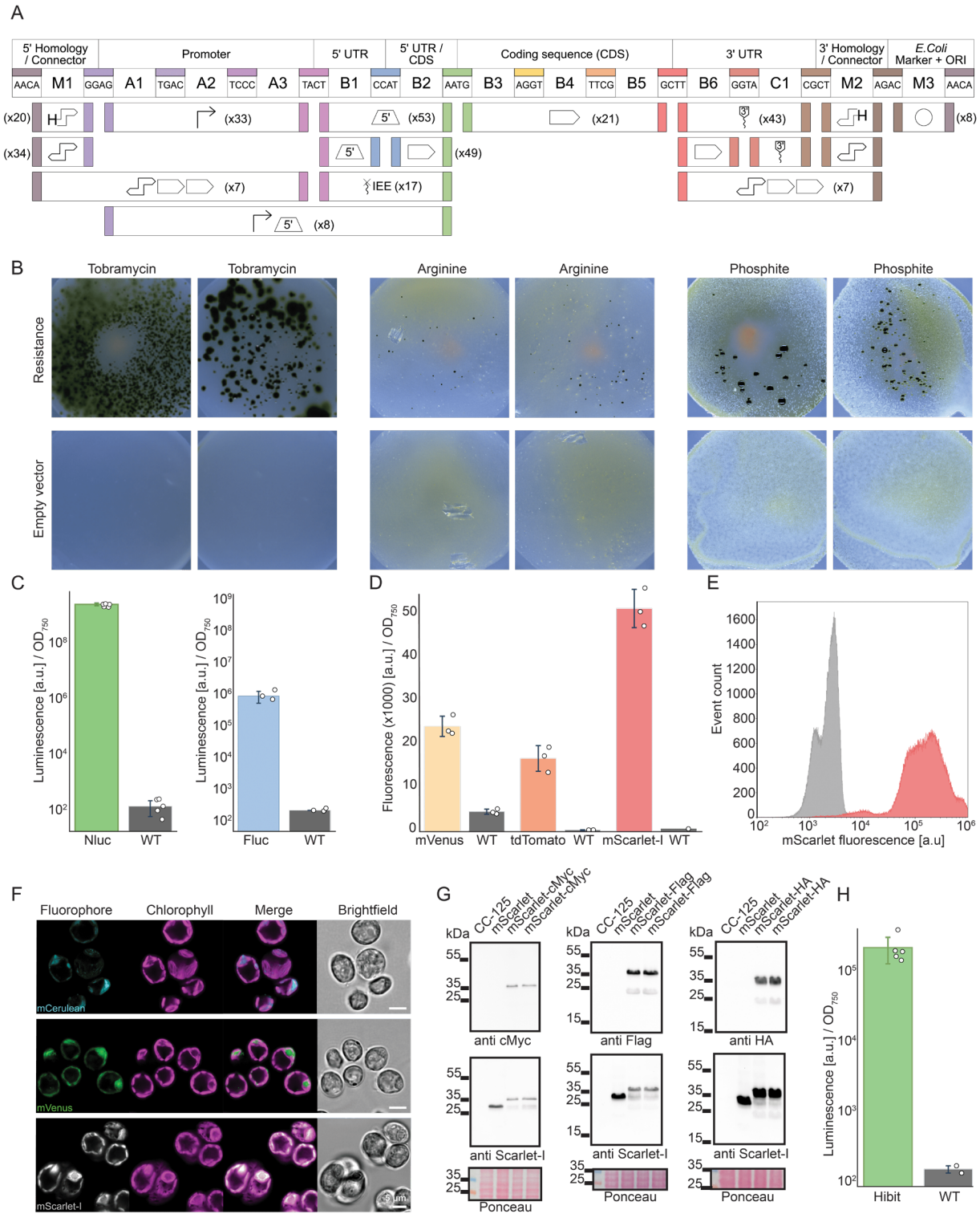

150

Figure 2: Establishing novel basic tools for chloroplast engineering. a, Architecture of the novel chloroplast modular cloning (MoClo) system and overview of the created genetic parts. The architecture follows the Phytobrick standard[47] and conserves the cloning overhangs of this system, as well as the nomenclature for the part types (A1-C1). The position M1-3 allow for higher modularity as reported by Stukenberg *et al.* Number of parts are indicated for each position **b,** Selection markers for chloroplast transformation. Three different selection marker systems are shown with two replicates and two negative controls for each one. Successful selection after chloroplast transformation can be observed for all three of them, notably with a high efficiency for tobramycin-based selection (100µg/mL). **c,** NanoLuc as a luminescence reporter for the chloroplast. Nanoluc signal of a transplastomic strain containing a NanoLuc expression cassette (green) is plotted as arbitrary units [a.u.] normalized to OD and compared to WT strain (gray). **d,** Novel fluorescent reporters for the chloroplast. Fluorescent signals of transplastomic strains containing different fluorescent reporter expression cassettes, measured via a plate reader, are plotted as arbitrary units [a.u.] normalized to OD_{750} and compared to WT strain (gray). **e,** Flow cytometry data of the transplastomic strain, containing a mScarlet-I expression cassette (red) compared to the WT strain (gray). **f,** Fluorescence microscopy images of the transplastomic strains containing different fluorophores (mCerluean, mVenus and mScarlet-I). **g,** Western blot analysis of transplastomic strains producing mScarlet FLAG-tagged, HA-tagged, cMyc-tagged in the C-term position. Each strain is also tested for the presence of mScarlet using mScarlet-I specific probes. Ponceau gels are shown for each gel. **h,** Nanoluc assay for the Hibit tag in C-term position. Data is plotted as arbitrary units [a.u.] normalized to OD_{750} and compared to WT strain (gray).

We also tested different luciferase-based and fluorescent reporters for the characterization and quantification of regulatory elements. As primary reporter, we identified NanoLuc luciferase (Extended Data Fig. 2a). This luminescence reporter did not interfere with chloroplast auto-fluorescence, and showed a high signal-to-noise ratio that was superior to that of established fluorescent reporters (Fig. 2c and 2d). Notably, it produced a luminescence signal that was nearly seven orders of magnitude higher than that of the wild-type background (Fig. 2c). As alternative to NanoLuc, we integrated the previously reported firefly luciferase[52] into our parts library. Furthermore, we tested four different fluorescent reporters (mVenus, mScarlet-I, td tomato and mCerulean), of which mScarlet-I performed best. This reporter showed little interference with chloroplast auto-fluorescence (Fig. 2d) and could be successfully applied in flow cytometry and microscopy (Fig. 2f). While the fluorescence of mCerulean measured in the plate reader was only 1.5 times higher (Extended Data Fig. 2b) than the wild-type signal on average, it was still sufficient to facilitate effective microscopy analysis (Fig. 2f).

Finally, we included additional parts for gene product detection into our library, which included modular tags (FLAG-, HA, cMyc-tags) for western blots and a HiBiT-luciferase complementation assay to tag and detect proteins of interest (Fig. 2g, h, Extended Data Fig2.e). This set of selection markers, reporter genes and regulatory parts provided the basis for all high-throughput characterization efforts and engineering applications of this study.

High-throughput characterization of regulatory elements

Having established the initial library of parts, we proceeded to systematically quantify the different regulatory parts using the NanoLuc based read-out. To that end, we tested various 5' untranslated regions (5'UTRs), as well as 3'UTRs, which both are known to significantly influence and regulate gene expression in the chloroplast.[53–56] Despite their cyanobacterial origins, chloroplasts diverge from their prokaryotic ancestors in gene expression regulation.[57] While prokaryotic gene expression is predominantly controlled at the transcriptional level, chloroplast gene expression is mainly regulated post-transcriptionally via RNA elements in the 5' and 3' UTRs.[58] Especially 5'UTRs are known to interact with chloroplast mRNA binding factors that regulate transcript maturation, stability and translation efficiency, thus determining gene expression levels.[59–63]

To test 5'UTRs, we constructed 35 different genetic constructs, each composed of the *rrn16* promoter, followed by a variable 5'UTR, the NanoLuc luciferase coding sequence, the *psbA* 3'UTR, and homology sequences for integration at the psbH locus, which is the most widely used integration site in *C. reinhardtii*. As 5'UTR, we used natural sequences sourced from *C. reinhardtii* and tobacco, as well as synthetic sequences. For each of the 35 designs, we picked 16 biological replicates, which we tested on two different growth media (TAP and HSM) and two different light conditions (light and dark). In total, this experiment involved the handling and analysis of 2,240 transplastomic strains.

The different transplastomic strains showed a broad luminescence, which spanned over more than three orders of magnitude (Fig. 3a). Strains carrying 5'UTRs of RNA polymerase and ribosomal proteins (*rpoC2, rlp16, rpl23*) showed on average lower expression levels, while strains carrying 5'UTRs of highly abundant proteins in photosynthesis (*rbcL*, *psaA, psbC*) showed high expression levels, aligning well with recently reported Ribo-seq data for Chlamydomonas.[64] These expression patterns proved to be consistent across the four different growth conditions, with the exception of the *petD* 5'UTR that somehow displayed divergent expression patterns across the two different media (Fig. 3b, (Extended Data Fig3.a-c).

Next, we focused on 3'UTRs. We constructed 36 different genetic constructs targeting the psbH locus, each carrying the *rrn16* promoter, the *psaA* 5'UTR, the NanoLuc luciferase coding sequence, and a variable 3'UTR, which we derived from *C. reinhardtii*, tobacco, or viral origin. Luminescence of the different transplastomic strains showed three levels of variability spanning across three orders of magnitude (Fig. 3c), low, medium and high, illustrating the relevance of 3'UTR on gene expression activity in chloroplasts, although to a lesser extent compared the 5'UTR.

224 Finally, we investigated intercistronic expression elements (IEEs) that are crucial for poly-
225 cistronic gene expression in the chloroplast. IEEs promote processing of polycistronic mRNAs
226 into stable monocistronic transcripts and protect these mRNAs against degradation[65,66] (Fig.
227 3d). Utilizing small RNA profiling data from the chloroplast of Chlamydomonas[20], we identified
228 15 potential candidates, which we tested as IEE between Firefly luciferase and NanoLuc
229 luciferase as reporter genes (Fig. 3e). With exception of three sequences (*trnF-psaC; rps18-*
230 *rps2; psbF-psbL*) all other sequence indicated successful processing into monocistronic
231 mRNAs. Interestingly, the different functional IEEs showed up to tenfold variation in luciferase
232 activity levels, highlighting the potential of these elements in modulating the expression of
233 stacked transgenes within the chloroplast (Fig. 3e). In summary, these experiments
234 established and quantified the behavior of more than 80 genetic elements in the chloroplast.

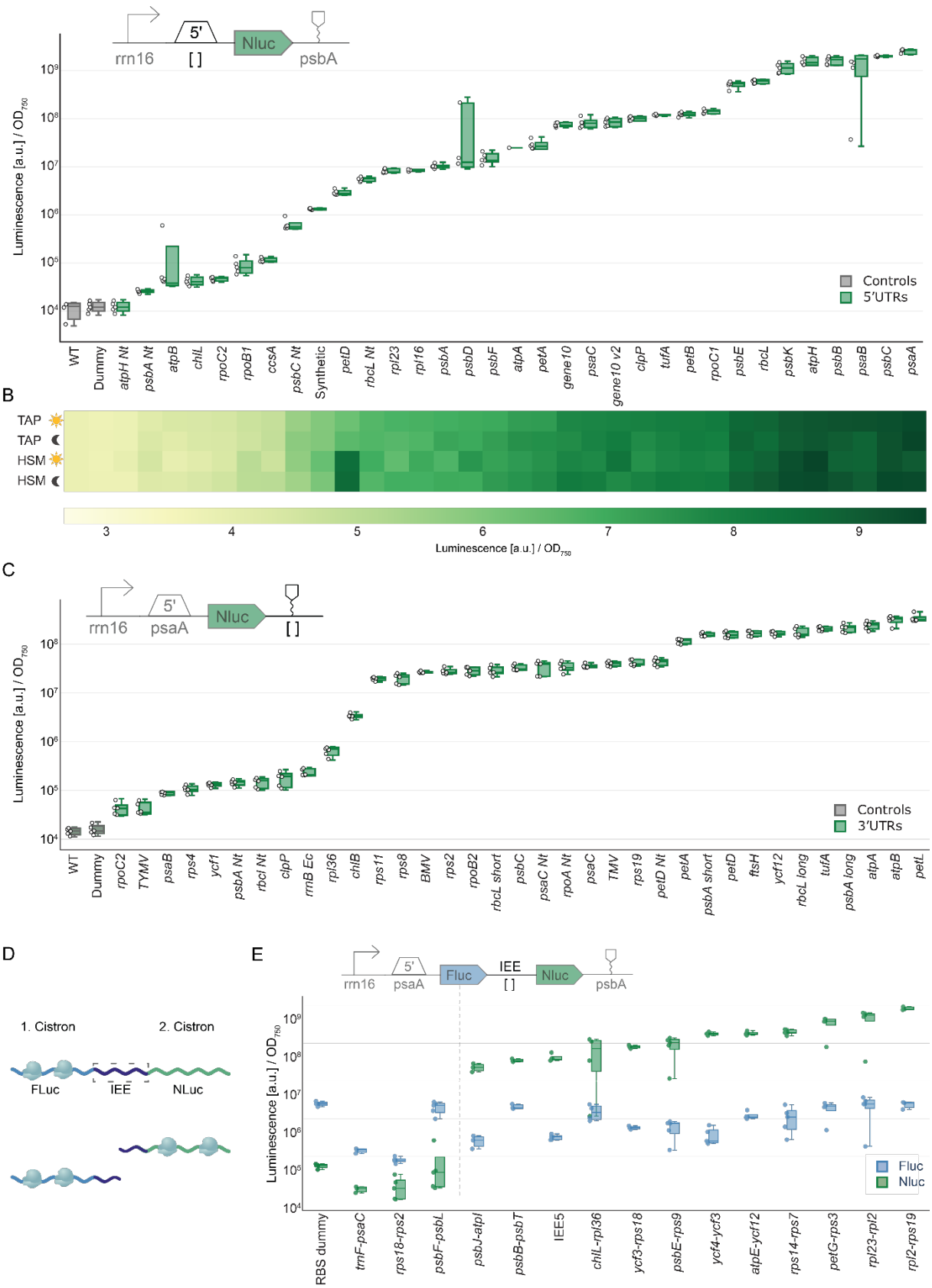

Figure 3: Characterization of regulatory parts for chloroplast gene expression. a, 5'UTR characterization 5'UTRs were characterized by measuring NanoLuc activity of transplastomic strains containing different constructs, which differ in their 5'UTR. Nanoluc signal of a transplastomic strain containing a NanoLuc expression cassette (green) is plotted as arbitrary units [a.u.] normalized to OD and compared to WT strain (gray). For all measurements, $n_{biological}$= 5, $n_{technical}$= 3. **b,** 5' characterization under four different conditions. Heatmap is showing the Nanoluc signal of transplastomic strains

under light, dark, TAP and HSM medium conditions. Similar expression patterns can be observed under all four conditions. **c,** 3'UTR characterization. 3'UTRs were characterized by measuring NanoLuc activity of transplastomic strains containing different constructs, which differ in their 3'UTR. Nanoluc signal of a transplastomic strain containing a NanoLuc expression cassette (green) is plotted as arbitrary units [a.u.] normalized to OD_{750} and compared to WT strain (gray). For all measurements, $n_{biological}$= 5, $n_{technical}$= 3 **d,** Function of Intercistronic expression elements (IEEs). Two cistrons are connected via an IEE. After processing via imported cis-factors, both cistrons are translated separately. **e,** IEE characterization. IEE characterization. IEEs were characterized by measuring NanoLuc and Fluc activity of transplastomic strains containing different constructs, which differ in their IEE. Luciferase signal of a transplastomic strain containing a NanoLuc expression cassette (green) is plotted as arbitrary units [a.u.] normalized to OD750 and compared to Fluc luminescence (blue). The dotted line differentiates IEEs with insufficient support for robust expression (left) from those facilitating strong expression (right). For all measurements, $n_{biological}$= 5, $n_{technical}$= 3.

Developing synthetic chloroplast expression elements through rational and library-based approaches

Most of the genetic elements tested thus far were of natural origin. Thus, we sought in the following to establish fully synthetic (i.e., non-native) genetic parts, in particular promoters. Inspired by the architecture of the *C. reinhardtii rrn16* promoter, we developed a minimal scaffold, consisting of only 46 base pairs carrying canonical -35 and -10 motifs. We preserved these -35 and -10 motifs across the majority of these promoters and modified the rest of the sequence to modulate expression strength and reduce the risk of unintended homologous recombination for multi-gene constructs.

In total, we rationally designed 21 different promoters and tested them in a standardized construct that was integrated at the psbH locus and included the different promoter sequences upstream of the psaA 5'UTR, the coding sequence of NanoLuc luciferase, and the psbA 3'UTR. The luminescence signal of the transplastomic strains varied across three orders of magnitude, suggesting that our synthetic promoters covered a range of different expression strengths (Fig. 4a).

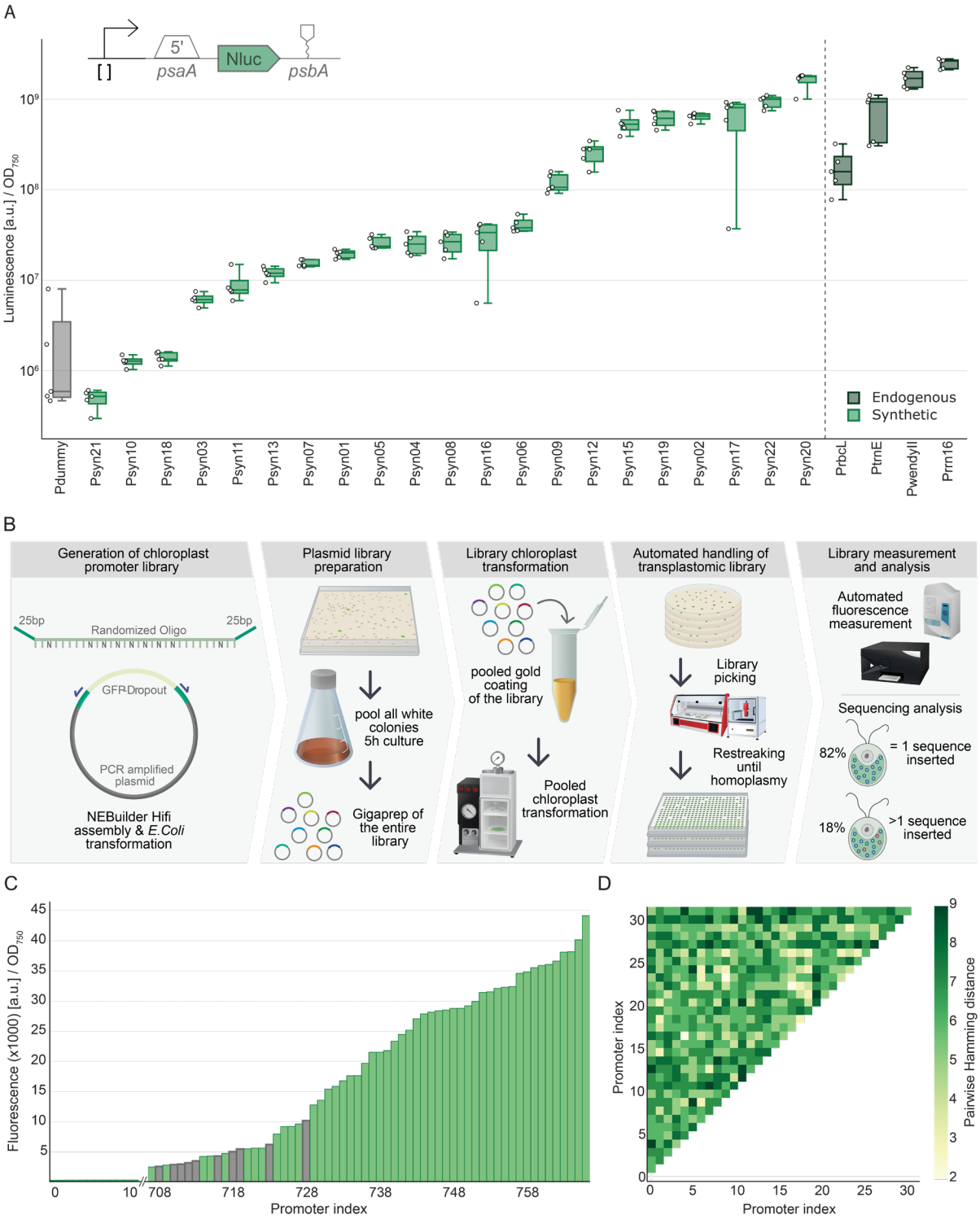

Figure 4: Designing and testing synthetic chloroplast promoters and library chloroplast transformation. **a,** Synthetic promoter characterization. Promoters were characterized by measuring NanoLuc activity of transplastomic strains containing different constructs, which differ in their promoters. Nanoluc signal of a transplastomic strain containing a NanoLuc expression cassette (green) is plotted as arbitrary units [a.u.] normalized to OD and compared to dummy sequence (gray). The dotted line demarcates synthetic promoters (left, light green) from endogenous ones (right, dark green). For all measurements, $n_{biological}$= 5, $n_{technical}$= 3. **b,** Conceptual workflow for transforming construct libraries into the chloroplast. Sequencing analysis showed that 82 % of transformants contained a single promoter variant and for 18% multiple sequence variants could be detected **c,** Fluorescence measurement of transplastomic promoter library. mScarlet-I fluorescence of the transplastomic strains containing different promoter variants was measured (Excitation 569 nm /Emission 605 nm). Fluorescence is plotted as arbitrary units [a.u.] normalized to OD $_{750}$. 768 transplastomic strains have been measured and a range of different mScarlet-I signals can be detected. Gray bars represent examples that were

281 selected in panel d for sequencing. **d**, Sequence analysis of sequenced transplastomic strains. Pairwise Hamming
282 distance is plotted for the promoter sequence variant, which was found in a set of 33 sequenced transplastomic strains.

283

284 Even though above experiments successfully identified synthetic promoters, we note that the
285 biolistic transformation remained a bottleneck in our automated workflow. This is, because
286 each of the 21 promoters that we tested required an individual transformation, limiting the total
287 number of promoter designs that could be assessed. To address this constraint, we explored
288 the feasibility of a pooled library approach, as opposed to transforming individual constructs.
289 As a proof of concept, we sought to transform and screen a library of degenerated promoter
290 sequences. This library was created by cloning a degenerated single strand oligonucleotide
291 into a pre-assembled vector containing a spectinomycin selection marker and an mScarlet
292 expression cassette (Fig. 4b). After the cloning step, colonies were pooled, the DNA of the
293 entire plasmid library was prepped and used for biolistic transformation. We selected 768
294 transformants that we systematically organized and screened via a fluorescent read-out. While
295 90% of the strains did show only little or no fluorescence, 10% showed a broad spectrum of
296 mScarlet fluorescence. We continued to characterize selected transformant strains in more
297 depth (Fig. 4c).

298 For that, we selected 32 individual strains and subjected them to sequencing. Using the
299 individual promoter sequences of the library as barcode enabled us to analyse, whether
300 individual sequence variants had been inserted or if a mixture of sequences persisted across
301 the genome copies. Of these 32 strains, 26 strains (82%) contained one unique sequence,
302 while the remaining six (18%) exhibited a mixture of sequences (Fig. 4d). Overall, these
303 findings did not only provide more than 20 additional synthetic promoter sequences for the
304 chloroplast, but notably also demonstrated the power of pooled library transformation in
305 chloroplasts, opening new possibilities for plastid synthetic biology and engineering.

306

307 Prototyping the effect of different genetic contexts on transgene expression

308 In all prior experiments, the different genetic elements were always assessed in the same
309 genetic context, that is within the same transcription unit (and at one specific integration site),
310 varying only one parameter (e.g., either promoter, 5'UTR, or 3'UTR). While this setup was
311 helpful to study the individual behavior of the respective elements that were tested, for more
312 advanced engineering approaches a collection of orthogonal part combinations are required
313 that are unique in their respective sequence and can be utilized together in multi-transgene
314 expression without the risk of unintended homologous recombination.

315 To prototype such orthogonal part combinations, we devised 11 unique combinations, all
316 expressing the NanoLuc reported, but each varying in promoter, 5'UTR, and 3'UTR (Fig. 5a).

317 In these experiments, the luminescence of the different combinations spanned three orders of
318 magnitude, indicating a broad range of expression strength. In almost all cases, expression
319 strength was correlated with expected 5'UTR activity (and promoter activity), with exception
320 of the *SynP9:rbcL:petA* and *SynP17:clpP:ycf12* constructs, whose expression strength
321 seemed to be rather correlated with expected promoter activity.
322

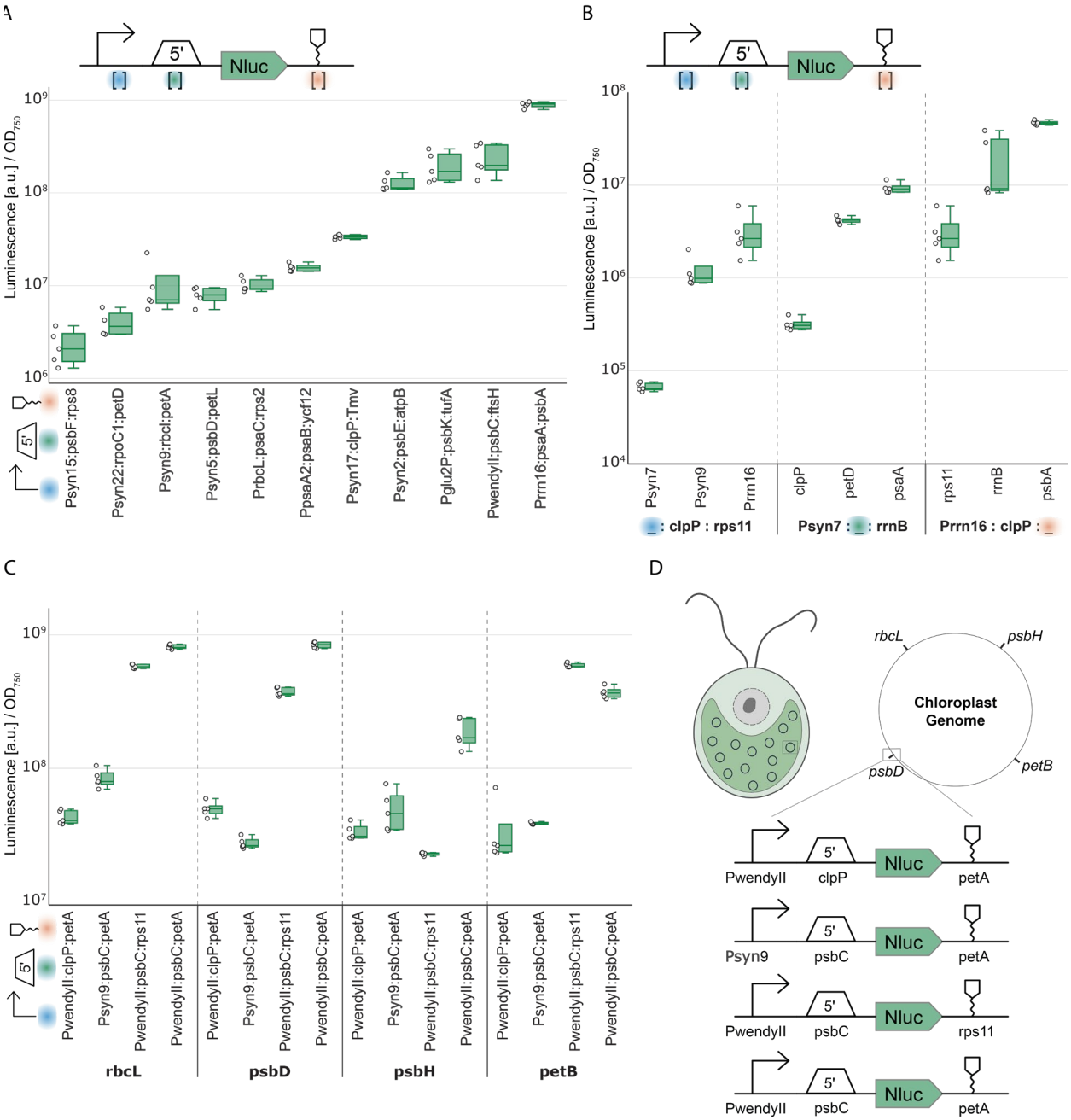

323

324 **Figure 5 Characterizing the effects of different genetic contexts**

325 **a,** Characterizing various combinations of parts. Combinations were characterized by measuring NanoLuc activity of
326 transplastomic strains containing different constructs, which differ in their promoters, 5'UTRs and 3'UTRs. For clarity
327 across the figure, part combinations are denoted as follows: Promoters by blue dots, 5'UTRs by green dots, and 3'UTRs
328 by orange dots. Nanoluc signal of a transplastomic strain containing a NanoLuc expression cassette (green) is plotted as
329 arbitrary units [a.u.] normalized to OD. For all measurements $n_{biological}$= 5, $n_{technical}$= 3. A range of three orders of magnitude

of NLuc signal can be observed. **b,** Characterizing parts in weak expression backgrounds. Combinations were characterized by measuring NanoLuc activity of transplastomic strains containing different constructs, which differ in their promoters, 5'UTRs and 3'UTRs. Nanoluc signal of a transplastomic strain containing a NanoLuc expression cassette (green) is plotted as arbitrary units [a.u.] normalized to OD. For all measurements $n_{biological}$= 5, $n_{technical}$= 3. A range of two orders of magnitude of NLuc signal can be observed. **c,** Characterizing the effect of different sites of integration across the chloroplast genome integration sites were characterized by measuring NanoLuc activity of transplastomic strains containing different constructs, containing 4 different combinations of parts integrated in 4 different locations in the chloroplast genome. **d,** Conceptual design of the characterization of different integration sites. Four different constructs, which vary in the promoter, 5'UTR and 3'UTR are integrated in four different locations of the chloroplast genome.

To study the context-dependency of individual genetic elements in more detail, we next devised a series of combinatorial constructs. This series included constructs, in which three different promoters of low-, medium-, and high-activity were tested in combination with low-activity elements clpP (5'UTR) and rps11 (3'UTR); three different 5'UTRs of low-, medium-, and high-activity were tested in context with the low-level activity promoter Psyn7 and the low-level activity 3'UTR rps11, respectively; and three different 3'UTRs of low-, medium-, high-activity were tested together with the high-activity promoter Prrn16 and the low-activity 5'UTR clpP. In all cases, the elements behaved as expected by increasing expression strength by approximately 10-fold and 50-fold for the medium- and high-activity element, confirming their functionality across different genetic contexts (Fig. 5b).

Finally, we also studied the impact of different integration sites within the chloroplast genome. To this end, we created four different transcriptional units (two of low and two of high transgene expression strength) that we integrated into four distinct locations (Fig. 5d, (Extended Data Fig. 4) within the chloroplast genome (psbH, rbcL, psbD, petB). For the rbcL, psbD, and petB integration sites we observed comparable expression levels between the four constructs (Fig. 5c). However, for the psbH integration site, we noted some differences, particularly for the construct containing the rps11 3'UTR. This observation is in line with a recent report that the 3'UTR at the psbH site is important in controlling read-through activity of neighboring genes, which in turn can modulate transgene expression.[67] Overall, these experiments showed that most constructs behaved similar independent of their genomic position, but also highlighted that validating individual constructs at the psbH site is important for quantifying actual transgene expression strength.

Applying the tools to prototype novel chloroplast traits in *C. reinhardtii*

Finally, we used our plastome engineering toolkit to demonstrate the prototyping of novel metabolic traits in the chloroplast of *C. reinhardtii*. As case example, we sought of introducing a recently reported synthetic photorespiratory bypass[7] into the chloroplast that is based on

368 two enzymes: glycolate dehydrogenase (GDH) and malate synthase (MS), respectively (Fig.
369 6a). These two enzymes cause the direct decarboxylation of the photorespiration product
370 glycolate into CO_2, which increases CO_2 concentrations in the chloroplast and was reported
371 to improve photosynthetic yield in different crops.[7,68]

372 As host for our engineering efforts, we chose a CO_2-concentrating mechanism deficient- and
373 glycolate dehydrogenase-deficient *C. reinhardtii* mutant (cc-5797, genotype confirmation in
374 Supplementary Fig. 2c-d) that shows a severe growth phenotype under atmospheric CO_2
375 concentrations due to increased photorespiration[69]. To express GDH and MS from the
376 chloroplast genome, we chose four regulatory elements and validated their activity at the psbH
377 integration site in cc-5797 using the NanoLuc reporter (Fig. 6b). We assembled the
378 transcriptional units for expression of GDH and MS, integrated these units into the psbH locus,
379 confirmed integration via colony PCR (Extended Data Fig. 5a) and verified the presence of
380 the malate synthase and the glycolate dehydrogenase through proteomics ((Extended Data
381 Fig. 5c). Interestingly, during our analysis, we detected functional expression of glycolate
382 dehydrogenase, indicating that the 5'UTR knock out of glycolate dehydrogenase was not
383 completely tight in the cc 5797 strain, suggesting that the growth phenotype was mainly
384 caused by deficiency of the CO_2-concentrating mechanism.

385 At 5% CO_2 concentration, the *C. reinhardtii* strain expressing MS and GDH and the negative
386 control (i.e., the cc 5797 strain expressing NanoLuc luciferase) behaved identical (Fig. 6d).
387 However, at ambient CO_2 concentrations, the strain with the functional photorespiration
388 bypass showed a clear growth benefit (Fig. 6c, Extended Data Fig. 5b). While both strains had
389 comparable doubling times (~43 hours), the strain expressing MS and GDH reached almost
390 two-fold higher final ODs, indicating that the pathway was functionally expressed from the
391 chloroplast (Fig. 6c, (Extended Data Fig5.b). Moreover, intracellular metabolomics unraveled
392 distinct differences between the engineered and the control strain. In the engineered strain,
393 intracellular glycolate concentrations (as well as the derived amino acids glycine and serine)
394 were significantly decreased compared to the control strain (Fig. 6e). In contrast, the levels of
395 pyruvate and energy metabolites, such as ATP were not significantly different between the
396 two strains (Fig. 6e), supporting the hypothesis that expression of MS and GDH had re-
397 channeled photorespiration flux towards the synthetic glycolate metabolism. Together, these
398 results demonstrated the general possibility to prototype novel metabolic traits, such as
399 improved photorespiration, in the chloroplast of *C. reinhardtii.*

400

401

402

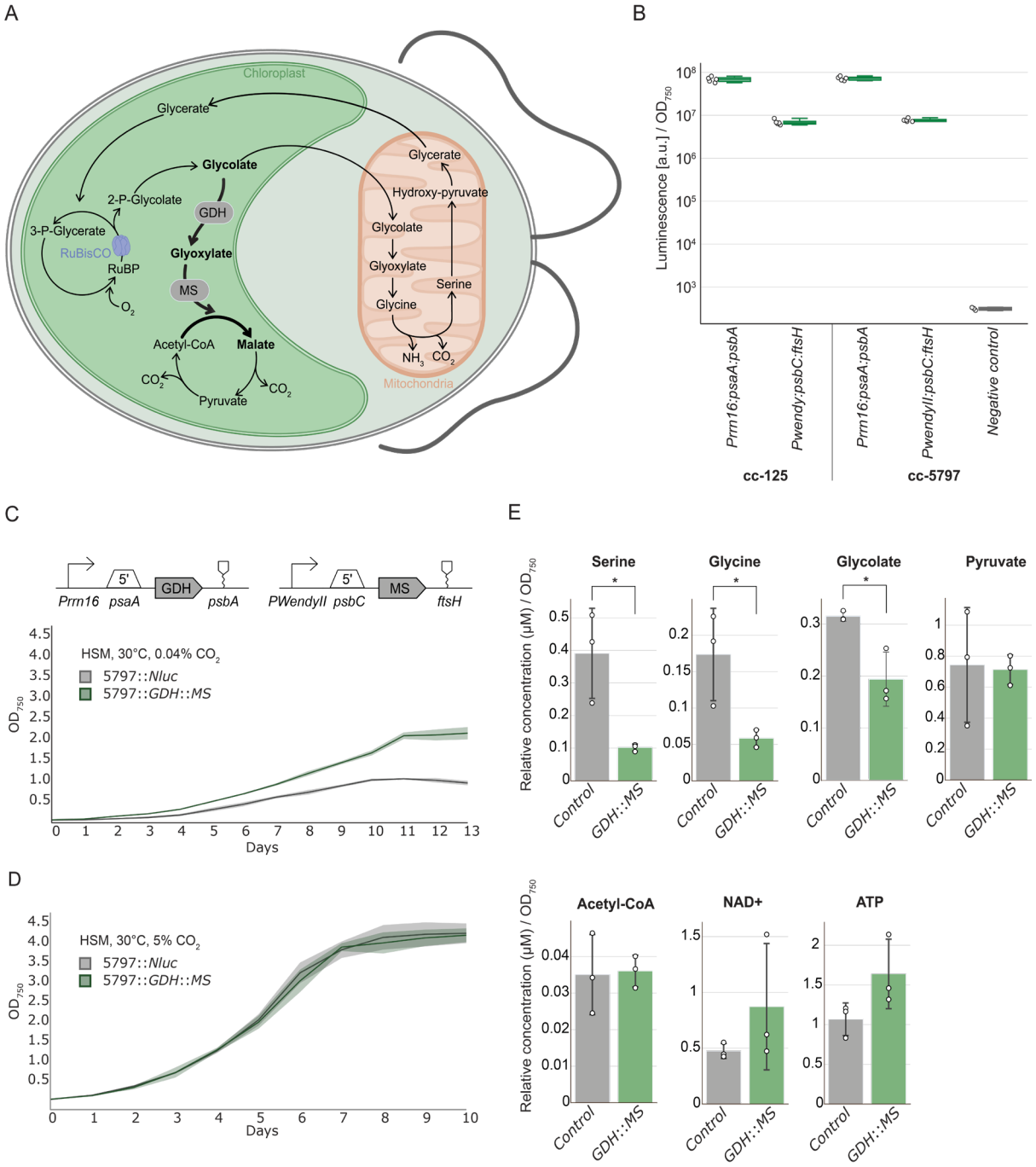

Figure 6 Introducing a synthetic photorespiratory bypass in the chloroplast of *C. reinhardtii*

a, Metabolic scheme for the previously reported synthetic photorespiration bypass. The pathway relies on the introduction of two genes (in gray): the glycolate dehydrogenase (GDH) and malate synthase (MS). **b,** Nanoluc assay for part combinations characterization in the cc-125 WT and cc-5797 mutant. Nanoluc signal is plotted as arbitrary units [a.u] normalized to OD_{750} and compared to the control-lacking reporter (in gray). For all measurements, $n_{biological}$=5. **c-d**, Growth curve of engineered strains and control at ambient CO2 and 5% CO2 respectively, shown as OD_{750} over time (days). Parts tested in b were used to express both GDH and MS. Engineered strains (5797::GDH::MS,in green) reach a two-fold final OD over the control strains (5797::Nluc) in ambient CO2 but behave similarly in 5% CO2. $n_{biological}$=3 for each curve. **e.** Intracellular metabolome analysis of engineered and control strains during the exponential growth phase. Relative concentrations (µM/OD_{750}) of serine, glycine, glycolate, pyruvate, acetyl-CoA, NAD+ and ATP are displayed for the 5797::GDH::MS (in green) and 5797::Nluc (in gray). $n_{biological}$=3 for each experiment. Significant changes are indicated by a * for a p_value<0.05. (serine, p_value = 0.023. glycine, p_value = 0.037. glycolate, p_value = 0.017).

416 # Discussion

417 Harnessing the full potential of synthetic biology in photosynthetic eukaryotes (and plant
418 systems in particular) necessitates considerable improvements in genetic engineering
419 capabilities, with chloroplasts emerging as a prime target for such efforts. Traditionally,
420 chloroplast engineering has been limited to a relatively small number of transplastomic strains
421 or plant lines, which has challenged a systematic characterization of genetic parts and more
422 complex constructs in chloroplasts.[32]

423 In this study we established *C. reinhardtii* as chloroplast model system, implemented an
424 automated workflow for the generation and handling of thousands transplastomic strains in
425 parallel, and introduced an extensive array of genetic tools to significantly advance the field of
426 chloroplast synthetic biology. By dramatically expanding the number of selection of markers,
427 reporter genes, and regulatory elements, our study paves the way for more ambitious
428 chloroplast engineering projects in *C. reinhardtii*. To facilitate a broader application and further
429 development within the community, all tools, including the 300 genetic parts are available
430 through repositories, and are already in use by other laboratories.[27] This set of parts provides
431 a first reference set that can be systematically extended in the future by more high-throughput
432 screens, including pooled library approaches, which have now become accessible for
433 chloroplasts through our efforts.

434 Our comprehensive toolkit enables multi-transgene expression through verified part
435 combinations, and offers the possibility for more advanced transgene stacking in the plastid
436 of *C. reinhardtii*. Thus, chloroplast-based strategies become a viable alternative for
437 applications targeting the chloroplast compared to nuclear genome-based efforts, which have
438 been used so far, but suffer from several disadvantages, such as low transgene expression
439 and gene silencing.[70,71] We demonstrate such an application by establishing a recently
440 reported synthetic photorespiration pathway[7] in *C. reinhardtii* chloroplasts that leads to a
441 twofold increase biomass yield under selection. This proof-of-concept provides new
442 possibilities for ongoing efforts to establish novel synthetic photorespiration pathways in
443 chloroplasts (e.g., the TaCo pathway[5] or BHAC cycle[8,9], or even replacing the Calvin cycle by
444 new-to-nature carbon fixation pathways (e.g., the Theta cycle[12] or reverse glyoxylate shunt.[72]

445 Despite some differences between the chloroplast of *C. reinhardtii* and land plants, the
446 plastome structure shows a high degree of conservation across photosynthetic eukaryotes.
447 Genetic elements from the chloroplast of *C. reinhardtii* have been successfully used in various
448 land plants, including tobacco[20], *Arabidopsis*[45], and poplar[43,44], and *vice versa* (e.g., as shown
449 in this study). This high degree of transferability lays the basis for the rapid testing and
450 optimization of genetic designs through our prototyping system, before a transfer of results to

land plants and crops. Especially when using high-throughput routines combined with pooled library strategies, these efforts could dramatically expand the search for new phenotypes and improved chloroplast functions, which could significantly contribute to developing climate-resilient crops, addressing agricultural challenges for an ever-growing world population facing climate change.

Materials and Methods

Escherichia coli Strains, Transformation, and Growth Conditions

Bacterial cultures during the cloning phase were incubated at 37°C in Luria-Bertani (LB) broth under shaking conditions for liquid cultures and on LB agar plates with 1.5% (m/V) agar for solid cultures. Antibiotic selection was applied according to the construction level: Chloramphenicol (34 µg/mL) for level 0 constructs (pME_Cp_UAV_GFP), Ampicillin (100 µg/mL) for level 1 (pME_Cp_0_7-8_003), and Kanamycin (50 µg/mL) for level 2 (pME_CP_0_7-8_006). Two chemically competent *E. coli* strains, DH10B and NEB Turbo, both sourced from New England Biolabs, were utilized for transformations, which were performed via heat shock as per the manufacturer's instructions. Plasmid DNA was isolated using Macherey-Nagel kits designed for both mini and midi preparations, the latter being essential for chloroplast transformation due to the supercoiled nature of the DNA obtained. Terrific Broth (TB) was employed to maximize yields in midi preparations.

Chlamydomonas reinhardtii Strains and Growth Conditions

Wild-type strains of *Chlamydomonas* were cultured on Tris-Acetate-Phosphate (TAP) medium in high light (~100 µmol photons m^{-2} s^{-1}), following the Chlamydomonas Resource Center's recipe, which included Hutner´s trace elements[73]. The medium was supplemented with Ampicillin (100-500 µg/mL) and Difco agar (Beckton Dickson, 0.8% m/V) for solid cultures. Transformations were performed on TAP agar plates supplemented with spectinomycin (100 µg/mL), tobramycin (100 µg/mL), or kanamycin (200 µg/mL) as required. Tobramycin antibiotic stocks have been prepared freshly every time. Transformed strains were propagated on TAP medium supplemented with Ampicillin (500 µg/mL) and an increasing concentration of either spectinomycin (100, 300, 500, 1000 µg/mL) or tobramycin (100, 150, 300 µg/mL) during the restreaking phase. Culture flasks were meticulously cleaned with detergent, rinsed thrice with deionized water, and autoclaved with Milli-Q water to eliminate any residual detergent (SOMAT). The study predominantly utilized the CC-125 mt+ mutant strain from the Chlamydomonas Resource Center, as well as cc-5797, a double mutant for Glycolate dehydrogenase and cia5, which is a global regulator for the CO_2 concentrating mechanism in *C. reinhardtii*.

For growth curves of cc-5797, pre-cultures were grown for 9 days in High Salt Medium, according to the Chlamydomonas Resource Center (HSM + $Spec_{100}$, 5% CO_2, 30°C) and used for inoculation of cultures at OD_{750}=0.05. Growth curves were carried in HSM supplemented with $Spec_{100}$, 0.04% CO_2, 30°C or HSM + $Spec_{100}$, 5% CO_2, 30°C for the control. 1 mL samples were taken every day and OD_{750} was measured.

492 **Chloroplast Transformation**

493 Chloroplast transformation in *Chlamydomonas* was executed using a Bio-Rad PDS/1000 He
494 (Bio-Rad) gene gun. Briefly, cells were grown in 50 mL TAP medium for two days before
495 inoculation into two 400 mL TAP cultures with 10-15 mL of the pre-culture. These cultures
496 were grown to a density of 10^7 cells/mL, harvested by centrifugation at 3000x g for 10 minutes,
497 and the pellets resuspended in 50 mL fresh TAP medium to disperse clumps before a second
498 centrifugation at 3000x g for 10 minutes. Pellets were resuspended in 10 mL TAP medium,
499 and 500 µL was used for plating on TAP agar plates supplemented with the appropriate
500 selection antibiotics. Plates were dried, uncovered, for at least one hour. 60 mg of gold
501 particles (0,6 µm Bio-Rad) was weighed and washed with 100µl 100% ethanol.
502 Subsequently gold particles were washed twice (1mL of water) and resuspended in 1mL of
503 water. 50µl of washed gold particles were coated with ~10 µg of supercoiled plasmid DNA
504 prepared via midi preparation for each construct, using 50µl of 2.5 M CaCl2 and 10µl 0.1 M
505 spermidine. All reagents were kept on ice throughout the protocol prevent particle clumping.
506 A pure ethanol wash was carried out, and DNA-bound gold beads were resuspended in 60µl
507 pure ethanol and used for biolistics, following Bio-Rad instructions. 1100 psi rupture disks
508 were used. Plates were incubated in the dark for recovery (~5-10 µmol photons m^{-2} s^{-1}) for
509 24h and moved to high light for selection (~100 µmol photons m^{-2} s^{-1}).

510

511 **Automated Picking, Re-streaking, and Re-arraying**

512 A PIXL robot (Singer Instruments) facilitated semi-automatic colony picking across various
513 array formats, including 96, 384, or 1536 configurations, with optimized parameters ensuring
514 consistent selection of *Chlamydomonas* colonies as outlined in the Supplementary Text 2. For
515 each construct, 16 colonies were selected when possible. The Rotor (Singer Instruments)
516 played a crucial role in managing arrays of transformants, adjusting antibiotic concentrations,
517 and preparing assay plates. It was employed for restreaking tasks and for dividing larger 384-
518 well plates into smaller 96-well measurement arrays, utilizing pin formats compatible with both
519 plate sizes.

520 **Part Design**

521 For our **Chl**amydomonas **Chloro**plast **Mod**ular **A**ssembly **S**ystem (CHLOROMODAS), we
522 employed the Phytobrick standard for the design of Level 0 parts[47], as previously utilized in
523 other plant and Chlamydomonas MoClo toolkits[37,46,74]. To assemble multiple transcription
524 units, we adapted the standard of the Marburg collection[75], with the exception of exchanging
525 the 3' Connector/Backbone Part overhang from AGCT to AGAC to enhance assembly
526 efficiency as determined by the NEB ligase fidelity tool.[76] All Level 0 parts were cloned into a
527 standard universal acceptor vector.
528 For the rational design of 5'UTR and 3'UTR Level 0 Parts, we utilized previously reported
529 RNA-seq and sRNA data[60] from C. reinhardtii chloroplasts for the annotation of transcription
530 start sites (TSS) and RNA-binding sites of trans-factors. Additionally, RNA secondary
531 structures of 3'UTRs were analyzed using ViennaRNA Web Services to identify necessary
532 stabilizing hairpin structures. The design of endogenous promoter parts involved examining
533 RNA-seq data to identify consensus -35 and -10 promoter sequences in the plastome prior to
534 the TSS. Suitable candidates for intercistronic expression elements (IEEs) were identified by
535 analyzing co-transcription data from a list of genes in the chloroplast and searching for RNA-
536 binding protein footprints within these sequences, indicating potential post-transcriptional
537 processing success.

538 Several parts in our toolkit underwent multiple design-build-test cycles using reporter gene
539 assays to determine the minimal sequence required for optimal function, such as for the rrn16
540 promoter and rbcL 3'UTR. Codon usage for coding sequences was optimized using the
541 Geneious codon optimization tool based on the chloroplast codon usage table for C. reinhardtii
542 (available at https://www.kazusa.or.jp). Original sequences for the glycolate dehydrogenase
543 (GDH) and malate synthase (MS) were sourced from South et al., 2019 and subsequently
544 optimized.
545 Level 0 parts were either amplified from the cc-125 genome or synthesized as fragments by
546 Twist Bioscience. Smaller parts (<100 bp) were cloned using annealed oligonucleotides.

547 **Part assembly**

548 Vectors and inserts were standardized to concentrations of 20 fmol. The assembly of Level 0
549 and Level 2 constructs utilized the type IIS restriction enzyme BsmBI, while BsaI was
550 employed for the assembly of Level 1 constructs. These assembly reactions were facilitated
551 using the NEBridge Golden Gate Assembly Kit from New England Biolabs for both BsaI and
552 BsmBI enzymes. The reaction mixtures, prepared without specifying volumes, included a
553 vector at 10 fmol, inserts at 20 fmol, the respective NEBridge Golden Gate Enzyme Mix (BsaI
554 or BsmBI), T4 DNA Ligase Reaction Buffer, and nuclease-free water to complete the mixture.
555 BsaI-based assembly reactions underwent 50 cycles of temperature alternations, with periods
556 at 37°C followed by cooling to 16°C. In contrast, BsmBI-based reactions alternated between
557 42°C and 16°C. The final steps for both methods involved a brief incubation at 60°C and a
558 final heat inactivation at 80°C before the transformation into competent bacterial cells (5µl of
559 the Golden Gate mixture).

560 **Fluorescence assays & FACS**

561 For chloroplast fluorescence analysis in *Chlamydomonas reinhardtii*, transformed and wild-
562 type (WT) colonies from 384-well arrays were resuspended in nuclease-free water in black
563 384-well Greiner Bio-One plates. Optical density (OD) was measured at 750 nm for
564 normalization. Fluorescence quantification utilized a microplate reader (Tecan infinite 200 Pro)
565 with specific settings for mScarlet-I (excitation: 569 nm, emission: 605 nm), mVenus
566 (excitation: 515 nm, emission: 545 nm), and tdTomato (excitation: 554 nm, emission: 585 nm).

567 FACS analysis was performed using a SONY SH800S Cell Sorter to assess fluorescent
568 protein expression. WT and mScarlet-I expressing strains underwent a two-day pre-culture
569 and a two-day culture in TAP medium, with spectinomycin (100 µg/mL) added for
570 transformants. Samples were diluted tenfold in TAP for optimal sorting. The SONY SH800S
571 settings were adjusted to accurately detect the fluorescent markers according to
572 manufacturer's instructions, which can be found in the Supplementary text 2.

573 **High-throughput pipeline for luminescence measurements**

574 To facilitate the high-throughput analysis of regulatory elements, a detailed pipeline was
575 established, as illustrated in Figure 1. This approach incorporated NanoLuc luciferase assays
576 from Promega for the quantitative assessment of regulatory element functionality. Initially,
577 transformants were propagated on 384-well agar plates. These plates were then segmented
578 into four 96-well solid-agar arrays with the aid of the Rotor robot, enhancing the biomass by
579 replicating each transformant into 5x5 squares. This cultivation extended over an 8-day period
580 to ensure adequate growth. Post-cultivation, colonies were carefully resuspended in 30 µL of
581 water within 384-well ECHO 525 plates (LABCYTE). Optical density (OD) measurements at
582 750 nm were conducted to ascertain cell density. To ensure standardized measurements
583 across seven replicates per construct, a custom Python pipeline was created. This pipeline
584 leverages a configuration file to set the liquid handling parameters for the ECHO 525 and
585 define experimental variables, including number of technical and biological replicates. The
586 objective was to achieve an OD_{750} of 0.01 for each replicate. To this end, the script uses the
587 previously measured absorbance data to generate pipetting instructions for the ECHO 525
588 liquid handler, which include automated modifications to the plate layout and the selection of
589 source wells. The dilutions were created in white 384-well plates, with alternate wells left
590 empty to minimize light interference between replicates in the subsequent luminescence
591 measurements. The luminescence assay was initiated by adding 10 µL of Nanoluc substrate
592 solution to each well. Following a 5-minute incubation at room temperature, luminescence was
593 measured using a plate reader. Afterwards, the data processing pipeline utilized a JSON
594 mapping file to link each measurement with the corresponding construct. By integrating the
595 ECHO pipetting instructions with the absorbance and luminescence data, a comprehensive
596 experiment overview was automatically compiled. This document includes normalized
597 luminescence values for each construct, corrected based on the OD_{750} measurements and
598 dilution factors to precisely reflect the activity of regulatory elements. This overview was
599 subsequently used for further analysis and data visualization.

600 **Metabolome extraction**

601 Daily 1 mL samples from the growth curve were mixed with an equal volume of 70% methanol
602 pre-cooled at -70°C, centrifuged, and the supernatant discarded before freezing the pellets at
603 -70°C. In a chemical fume hood and with proper PPE (gloves and glasses), 200 µL of 50%
604 methanol in TE buffer (10 mM Tris-HCl, 1 mM EDTA, pH 7.0) was added to each pellet.
605 Mechanical disruption was performed in a bead mill (Bead Bug) using 0.375 g of acid-washed
606 glass beads (500 µm) for two 30-second cycles at maximum power, with samples cooled on
607 ice between cycles. Following disruption, 200 µL of 100% chloroform was added, and the
608 mixture was vortexed for 30 seconds. After centrifugation at 13,000 xg for 10 minutes at -10°C,
609 the upper phase was extracted with 1 mL syringes, slowly filtered through PTFE filters into
610 pre-cooled Eppendorf tubes, and transferred into metabolomics vials for analysis, with careful
611 handling to avoid warming and contamination.

612 **Metabolome analysis**

613 Quantitative determination of the targets was performed using an LC-MS/MS system,
614 integrating chromatographic separation and mass spectrometry for precise analysis.
615 Chromatographic separation was achieved on an Agilent Infinity II 1290 HPLC system,
616 employing columns of varying specificities (Kinetex EVO C18, ZicHILIC SeQuant, and
617 SeQuant ZIC-pHILIC) with particle sizes ranging from 3 to 5 µm and pore sizes of 100 Å

618 (Phenomenex), connected to guard columns of similar specificity. The flow rates varied
619 between 0.1 and 0.3 mL/min, with mobile phases tailored to each experiment: CoA esters (1)
620 50 mM Ammonium Formate in water and 100% methanol, organic acids (2) 0.1% formic acid
621 in water and methanol, amino acids (3) 0.1% Formic acid in 99:1 water:acetonitrile and
622 acetonitrile:water, and ATP and NAD+ (4) 10 mM ammonium acetate in water and acetonitrile,
623 all adjusted to specific pH levels and temperatures. Injection volumes were set at 1 or 2 µL,
624 with mobile phase profiles designed to optimize separation over varying times and gradients.

625 Mass spectrometry analysis was conducted using an Agilent 6495 ion funnel mass
626 spectrometer, operating in both positive and negative ionization modes with specific settings
627 for ESI spray voltage, nozzle voltage, sheath gas temperature, nebulizer pressure, and drying
628 gas temperature to ensure optimal detection and quantification. Compounds were identified
629 and quantified based on their mass transition, retention time, and peak area, compared to
630 standards, using MassHunter software. Relative abundance and absolute concentrations
631 were determined based on peak areas and external standard curves, respectively. The
632 optimization of mass transitions, collision energies, cell accelerator voltages, and dwell times
633 was achieved using chemically pure standards, with the parameter settings detailed in
634 Supplementary Tables 1 through 4 for each experimental variation.

635 **Proteome extraction**

636 Cells were cultured in TAP medium for four days until reaching a density of 10^7 cells/mL or
637 exponential phase in a 50 mL pre-culture. Cultures was centrifuged at 3000x g for 10 minutes
638 at room temperature. The supernatant was removed, and the cell pellet was washed with 30
639 mM Tris-HCl (pH 7.9), followed by a second centrifugation. The pellet was then either used
640 immediately or stored at -80°C. Cell pellets were lysed by adding 500 µL of Tris-HCl with
641 protease inhibitors and 0.5 µg/µL lysozyme (Sigma-Aldrich), incubating at 25°C for 1 hour.
642 Then, 400 µL of 2% sodium deoxycholate (SDC) with 10 mM dithiothreitol (DTT) was added.
643 After three freeze-thaw cycles, the pellet was sonicated, heated at 90°C for 30-45 minutes,
644 and sonicated again. The lysate was centrifuged at 14,000x g for 30 minutes at 4°C, collecting
645 the supernatant for further processing. The supernatant was mixed with six volumes of cold (-
646 20°C) acetone and incubated overnight at -20°C. After centrifugation at 5000x g for 20 minutes
647 at 4°C, the supernatant was discarded. The pellet was washed twice with cold methanol, dried,
648 and reconstituted in 200 µL of 0.5% SDC. Protein concentration was determined using BCA
649 and pre-diluted BSA (Pierce BCA, Thermo Fischer Scientific) following manufacturer's
650 protocol, and 50 µg total protein was used for further protein purification by SP3[77] as described
651 previously with minor modifications. In short, proteins were bound to 4 µl SP3 beads (40% v/v)
652 in presence of 70 % acetonitrile for 15 min at room temperature, followed by two washes of
653 beads with 70 % Ethanol and an additional wash with acetonitrile. After removal of the
654 supernatant, 1 µg trypsin in 100 mM NH_4HCO_3 were added to the beads and digested shaking
655 overnight at 30°C. Following digest, beads were separated and peptides containing
656 supernatant was collected and further purified and desalted by C18-solid phase extraction
657 using Chromabound spin columns (Macherey-Nagel). Cartridges were prepared by adding
658 acetonitrile, followed by equilibration with 0.1% TFA. Acidified peptides were loaded on
659 equilibrated cartridges, washed with 5% ACN and 0.1% TFA containing buffer and finally
660 eluted with 50% ACN and 0.1% TFA.

661 **Proteome analysis**

662 Dried peptides were reconstituted in 0.1% Trifluoroacetic acid and then analyzed using liquid-
663 chromatography-mass spectrometry carried out on an Exploris 480 instrument connected to
664 an Ultimate 3000 RSLC nano and a nanospray flex ion source (all Thermo Scientific). Peptide
665 separation was performed on a reverse phase HPLC column (75 µm x 42 cm) packed in-
666 house with C18 resin (2.4 µm; Dr. Maisch). The following separating gradient was used: 94%
667 solvent A (0.15% formic acid) and 6% solvent B (99.85% acetonitrile, 0.15% formic acid) to
668 25% solvent B over 97 min., and an additional increase of solvent B to 35% for 35 min. at a
669 flow rate of 300 nl/min. MS raw data was acquired on an Exploris 480 (Thermo Scientific) in
670 data independent acquisition (DIA) mode. Peptides were ionized at a spray voltage of 2.3 kV,
671 ion transfer tube temperature set at 275 °C. The funnel RF level was set to 45. For DIA
672 experiments full MS resolutions were set to 120.000 at m/z 200 and full MS, AGC (Automatic
673 Gain Control) target was 300% with an IT of 50 ms. Mass range was set to 350-1200. AGC
674 target value for fragment spectra was set at 3000%. 60 windows of 4 Da were used with an
675 overlap of 1 Da (m/z range 550-678). Resolution was set to 15,000 and IT to 50 ms. Stepped
676 HCD collision energy of 27, 30, 32 % was used. MS1 data was acquired in profile, MS2 DIA
677 data in centroid mode. Analysis of DIA data was performed using the DIA-NN version 1.8[78] a
678 uniprot protein database from *Chlamydomonas reinhardtii* with additionally added sequences
679 to generate a data set specific spectral library for the DIA analysis. The neural network based
680 DIA-NN suite performed noise interference correction (mass correction, RT prediction and
681 precursor/fragment co-elution correlation) and peptide precursor signal extraction of the DIA-
682 NN raw data. The following parameters were used: Full tryptic digest was allowed with two
683 missed cleavage sites, and oxidized methionines and carbamidomethylated cysteins. Match
684 between runs and remove likely interferences were enabled. The precursor FDR was set to
685 1%. The neural network classifier was set to the single-pass mode, and protein inference was
686 based on genes. Quantification strategy was set to any LC (high accuracy). Cross-run
687 normalization was set to RT-dependent. Library generation was set to smart profiling. DIA-NN
688 outputs were further evaluated using the SafeQuant[79,80] script modified to process DIA-NN
689 outputs

690 **Immunoprecipitation analysis**

691 For protein analysis via SDS-PAGE, samples were prepared by centrifuging 8 ml of culture
692 with 4.10^7 cells at 4500 rpm and 4°C for 2 minutes, decanting the supernatant, and
693 resuspending the cells in the remaining medium for transfer to 1.5 ml Eppendorf tubes. After
694 a subsequent centrifugation for 30 seconds at 4°C, the supernatant was removed, and cells
695 were resuspended in 120 µl of 0.1 M Na2CO3 carbonate buffer, followed by the addition of
696 110 µl of 5% SDS solution. Samples were then mixed vigorously, heated at 95°C for 45
697 seconds, snap-frozen in liquid nitrogen, and stored at -20°C.

698 Protein concentrations were determined using the Lowry assay. Solutions A and B for the
699 Lowry assay were prepared and mixed, stored at 4°C. Protein standards were prepared by
700 diluting 1 mg/ml BSA in ddH2O, and samples were prepared from the -20°C freezer, with
701 triplicates of 90 µl water and 10 µl supernatant. After adding 1 ml of Lowry's solution and
702 incubating for 15 minutes at 25°C, 100 µl of 1x Folin reagent was added, and samples were
703 incubated for an additional 20 minutes. Absorbance was measured at λ = 750 nm to determine
704 protein concentrations.

705 SDS-gel electrophoresis was performed using prepared solutions for stacking (3%) and
706 separating (10%) gels. Gels were assembled, polymerized, and loaded with samples prepared
707 with 30 µg of protein in a final volume of 60 µl, including 4x loading buffer. Electrophoresis
708 was conducted at 160 V until the chlorophyll was about to exit the gel. Subsequently, samples
709 were prepared for Western blotting using Whatman paper and nitrocellulose membranes. The
710 membranes were blocked with 5% non-fat dry milk in TBST (20 mM Tris, 150 mM NaCl, 0.1%
711 Tween-20) for 1 hour at room temperature and incubated overnight at 4°C with primary
712 antibodies specific to the target tag : HA tag, mouse monoclonal antibody (Sigma). FLAG,
713 mouse monoclonal antibody (Sigma). Myc, mouse monoclonal antibody (Invitrogen).
714 Following primary antibody incubation, membranes were washed three times with TBST and
715 secondary antibodies for 1 hour at room temperature and proteins were analyzed using a gel
716 imager.

717 **Data analysis, plotting and statistical analysis**

718

719 Data analysis and visualization were performed using Python 3.10.5. For parsing and
720 processing, the pandas library (version 1.4.3) was utilized. Visualization of the data was
721 conducted using the Plotly library (version 5.9.0). Data is displayed as box plots and adjacent
722 individual data points on decadic logarithm scale. The midlines of the box plots represent the
723 median, the boxes' upper and lower limits represent the 1st and 3rd quartiles. Whiskers
724 correspond to the box' edges +/- 1.5 times the interquartile range.

725 Bar graphs, specifically in Figures 2 and 6, depicted mean values with error bars indicating
726 standard deviation, providing a clear visual summary of the data's central tendency and
727 variability. For the analysis of fluorescence-activated cell sorting (FACS) data, the FlowCal
728 library (version 1.3.0) was employed, presenting data on a logicle scale, a method detailed in
729 the provided reference.[81]

730 Metabolomics data underwent statistical examination using the scipy library (version 1.8.1).
731 The significance of these analyses was based on unpaired t-tests. Growth curve data were
732 visualized using mean values with shading to represent the standard error. Doubling times for
733 each strain were calculated using GraphPad Prism 10 and its Exponential (Malthusian) Growth
734 function, providing the doubling time over the first 7 days (exponential phase).

735 **Fluorescence microscopy**

736 For imaging, cells were grown to exponential phase (2-8x10^6 cells mL^{-1}) in TAP media. 10 µL
737 of cell suspension was overlaid with 30 µL of 1% TP-low-melting point agarose in µ-Slide 18
738 Well chambered coverslips (ibidi, Germany). All fluorescence images were captured using a
739 Zeiss LSM880 confocal microscope in Airyscan mode using a 63x 1.4 numerical aperture (NA)
740 Plan-Apo oil-immersion lens (Carl Zeiss, Germany). Brightfield images were captured using
741 the microscope T-PMT output channel. Specific settings are given in Supplementary text 1.

742 **Colony PCR analysis**

743 Chlamydomonas strains were subjected to colony PCR analysis. The cells were processed in
744 384 Greiner PCR plates, each well containing 25 µL of an extraction buffer composed of 10
745 mM Tris, 5 mM EDTA, and 0.01% Triton100, adjusted to pH 8. The plates underwent vortexing,
746 followed by a boiling step at 100°C for 10 minutes. Subsequently, the plates were vortexed
747 again and then cooled on ice for 5 minutes before centrifugation. The supernatant obtained
748 from this process was diluted in a 1:5 ratio with the extraction buffer and used as the DNA
749 template for PCR reactions.

750 For the PCR amplification, the 384 Greiner PCR plates were prepared by adding 0,5µL of
751 primer (10 µM) to each well, followed by 8 µL of Phusion High Fidelity Master mix (New
752 England Biolabs) according to the manufacturer's instructions. These steps were facilitated
753 using the ECHO 525 liquid handling system. To this mixture, 1 µL of the 1:5 diluted DNA
754 template was added. The PCR reaction was then performed as per the manufacturer's
755 guidelines, with the annealing temperature being adjusted based on the specific primer
756 combination used. GeneRuler 1kb DNA ladder (Thermo Fischer Scientific) was used for every
757 gel shown in the study. cPCR confirming Nanoluc insertion in each strain used for part
758 characterization can be found in Supplementary Fig1 and 2.

759

760 **Design, construction, and chloroplast transformation of a degenerated promoter**
761 **library**

762

763 A 90 bp single stranded degenerated oligo was designed and ordered. This oligo has 25bp
764 homologies at the 5' and 3' end to an already pre-assembled vector. The oligo also contains
765 40 bp of the core *rrn16* promoter, but with 9 sites which are changed to a degenerated base
766 pair. The pre-assembled vector contains a spectinomycin resistance and a mScarlet-I
767 expression cassette, consisting of a *psaA* 5'UTR, the mScarlet-I coding sequence, the *psbA*
768 3'UTR and 5'and 3' homology flanks for the integration in the *psbH* locus. The vector was then
769 PCR amplified and subsequently used for the NEB HiFi assembly together with the
770 degenerated oligo. Afterwards all red colonies were pooled in 500mL of TB medium. After 5
771 hours of incubation, the DNA of the entire library was isolated via the NucleoBond Xtra Maxi
772 Kit (Macherey Nagel). This pooled DNA-isolation was used for the subsequent chloroplast by
773 coating the plasmid mixture on the gold nanoparticles. After the chloroplast transformation,
774 768 colonies were picked and restreaked 4 times (once a week) to reach homoplasmy.
775

776 Data availability

777 Raw mass spectrometry data, as well as annotated plasmid maps will be submitted to the
778 "Edmund" Max Planck Society open-source database, as well as deposited in GenBank.

779 Code availability

780 The automation and data analysis scripts as well as the genbank files of all the plasmids
781 used in this study (including the entire chloroplast MoClo collection) are available at
782 https://github.com/ChlamyMarburg/ChloroplastTools

783

784

785 # References

786 1. Wurtzel, E. T. *et al.* Revolutionizing agriculture with synthetic biology. *Nat. Plants* **5**,
787 1207–1210 (2019).
788 2. Archibald, B. N., Zhong, V. & Brophy, J. A. N. Policy makers, genetic engineers, and an
789 engaged public can work together to create climate-resilient plants. *PLOS Biol.* **21**,
790 e3002208 (2023).
791 3. Qi, B. *et al.* Production of very long chain polyunsaturated omega-3 and omega-6 fatty
792 acids in plants. *Nat. Biotechnol.* **22**, 739–745 (2004).
793 4. Ye, X. *et al.* Engineering the Provitamin A (β-Carotene) Biosynthetic Pathway into
794 (Carotenoid-Free) Rice Endosperm. *Science* **287**, 303–305 (2000).
795 5. Scheffen, M. *et al.* A new-to-nature carboxylation module to improve natural and synthetic
796 CO2 fixation. *Nat. Catal.* **4**, 105–115 (2021).
797 6. Trudeau, D. L. *et al.* Design and in vitro realization of carbon-conserving photorespiration.
798 *Proc. Natl. Acad. Sci.* **115**, E11455–E11464 (2018).
799 7. South, P. F., Cavanagh, A. P., Liu, H. W. & Ort, D. R. Synthetic glycolate metabolism
800 pathways stimulate crop growth and productivity in the field. *Science* **363**, eaat9077
801 (2019).
802 8. Schada von Borzyskowski, L. *et al.* Marine Proteobacteria metabolize glycolate via the β-
803 hydroxyaspartate cycle. *Nature* **575**, 500–504 (2019).
804 9. Roell, M.-S. *et al.* A synthetic C4 shuttle via the β-hydroxyaspartate cycle in C3 plants.
805 *Proc. Natl. Acad. Sci.* **118**, e2022307118 (2021).
806 10. Kebeish, R. *et al.* Chloroplastic photorespiratory bypass increases photosynthesis
807 and biomass production in Arabidopsis thaliana. *Nat. Biotechnol.* **25**, 593–599 (2007).
808 11. Schwander, T., Schada von Borzyskowski, L., Burgener, S., Cortina, N. S. & Erb, T.
809 J. A synthetic pathway for the fixation of carbon dioxide in vitro. *Science* **354**, 900–904
810 (2016).

811 12. Luo, S. *et al.* Construction and modular implementation of the THETA cycle for
812 synthetic CO2 fixation. *Nat. Catal.* **6**, 1228–1240 (2023).
813 13. Yu, H., Li, X., Duchoud, F., Chuang, D. S. & Liao, J. C. Augmenting the Calvin–
814 Benson–Bassham cycle by a synthetic malyl-CoA-glycerate carbon fixation pathway. *Nat.*
815 *Commun.* **9**, 2008 (2018).
816 14. Luo, S. *et al.* A cell-free self-replenishing CO2-fixing system. *Nat. Catal.* **5**, 154–162
817 (2022).
818 15. Bar-Even, A. Daring metabolic designs for enhanced plant carbon fixation. *Plant Sci.*
819 **273**, 71–83 (2018).
820 16. Zhu, X.-G., Ort, D. R., Parry, M. A. J. & von Caemmerer, S. A wish list for synthetic
821 biology in photosynthesis research. *J. Exp. Bot.* **71**, 2219–2225 (2020).
822 17. Wichmann, J. *et al.* Farnesyl pyrophosphate compartmentalization in the green
823 microalga Chlamydomonas reinhardtii during heterologous (E)-α-bisabolene production.
824 *Microb. Cell Factories* **21**, 190 (2022).
825 18. Lu, Y., Rijzaani, H., Karcher, D., Ruf, S. & Bock, R. Efficient metabolic pathway
826 engineering in transgenic tobacco and tomato plastids with synthetic multigene operons.
827 *Proc. Natl. Acad. Sci.* **110**, E623–E632 (2013).
828 19. Schindel, H. S., Piatek, A. A., Stewart, C. N. & Lenaghan, S. C. The plastid genome
829 as a chassis for synthetic biology-enabled metabolic engineering: players in gene
830 expression. *Plant Cell Rep.* **37**, 1419–1429 (2018).
831 20. Fuentes, P. *et al.* A new synthetic biology approach allows transfer of an entire
832 metabolic pathway from a medicinal plant to a biomass crop. *eLife* **5**, e13664 (2016).
833 21. Lu, Y. *et al.* Horizontal Transfer of a Synthetic Metabolic Pathway between Plant
834 Species. *Curr. Biol.* **27**, 3034-3041.e3 (2017).
835 22. Long, B. M. *et al.* Carboxysome encapsulation of the CO2-fixing enzyme Rubisco in
836 tobacco chloroplasts. *Nat. Commun.* **9**, 3570 (2018).
837 23. Chen, T. *et al.* Engineering α-carboxysomes into plant chloroplasts to support
838 autotrophic photosynthesis. *Nat. Commun.* **14**, 2118 (2023).

24. Fei, C., Wilson, A. T., Mangan, N. M., Wingreen, N. S. & Jonikas, M. C. Modelling the pyrenoid-based CO2-concentrating mechanism provides insights into its operating principles and a roadmap for its engineering into crops. *Nat. Plants* **8**, 583–595 (2022).

25. Atkinson, N., Mao, Y., Chan, K. X. & McCormick, A. J. Condensation of Rubisco into a proto-pyrenoid in higher plant chloroplasts. *Nat. Commun.* **11**, 6303 (2020).

26. Nam, O. *et al.* A Protein Blueprint of the Diatom CO2-Fixing Organelle. 2023.10.26.564148 Preprint at https://doi.org/10.1101/2023.10.26.564148 (2023).

27. Barrett, J. *et al.* A promiscuous mechanism to phase separate eukaryotic carbon fixation in the green lineage. 2024.04.09.588658 Preprint at https://doi.org/10.1101/2024.04.09.588658 (2024).

28. He, S., Crans, V. L. & Jonikas, M. C. The pyrenoid: the eukaryotic CO2-concentrating organelle. *Plant Cell* **35**, 3236–3259 (2023).

29. Barrett, J., Girr, P. & Mackinder, L. C. M. Pyrenoids: CO2-fixing phase separated liquid organelles. *Biochim. Biophys. Acta BBA - Mol. Cell Res.* **1868**, 118949 (2021).

30. Adler, L. *et al.* New horizons for building pyrenoid-based CO2-concentrating mechanisms in plants to improve yields. *Plant Physiol.* **190**, 1609–1627 (2022).

31. Bock, R. Genetic engineering of the chloroplast: novel tools and new applications. *Curr. Opin. Biotechnol.* **26**, 7–13 (2014).

32. Boehm, C. R. & Bock, R. Recent Advances and Current Challenges in Synthetic Biology of the Plastid Genetic System and Metabolism. *Plant Physiol.* **179**, 794–802 (2019).

33. Ramundo, S., Rahire, M., Schaad, O. & Rochaix, J.-D. Repression of Essential Chloroplast Genes Reveals New Signaling Pathways and Regulatory Feedback Loops in Chlamydomonas. *Plant Cell* **25**, 167–186 (2013).

34. Esland, L., Larrea-Alvarez, M. & Purton, S. Selectable Markers and Reporter Genes for Engineering the Chloroplast of Chlamydomonas reinhardtii. *Biology* **7**, 46 (2018).

35. Dauvillee, D., Hilbig, L., Preiss, S. & Johanningmeier, U. Minimal Extent of Sequence Homology Required for Homologous Recombination at the psbA Locus in

867 Chlamydomonas reinhardtii Chloroplasts using PCR-generated DNA Fragments.
868 *Photosynth. Res.* **79**, 219–224 (2004).
869 36. Frangedakis, E. *et al.* Construction of DNA Tools for Hyperexpression in Marchantia
870 Chloroplasts. *ACS Synth. Biol.* **10**, 1651–1666 (2021).
871 37. Occhialini, A. *et al.* MoChlo: A Versatile, Modular Cloning Toolbox for Chloroplast
872 Biotechnology. *Plant Physiol.* **179**, 943–957 (2019).
873 38. Jackson, H. O., Taunt, H. N., Mordaka, P. M., Smith, A. G. & Purton, S. The Algal
874 Chloroplast as a Testbed for Synthetic Biology Designs Aimed at Radically Rewiring Plant
875 Metabolism. *Front. Plant Sci.* **12**, (2021).
876 39. Li, X. *et al.* A genome-wide algal mutant library and functional screen identifies genes
877 required for eukaryotic photosynthesis. *Nat. Genet.* **51**, 627–635 (2019).
878 40. Fauser, F. *et al.* Systematic characterization of gene function in the photosynthetic
879 alga Chlamydomonas reinhardtii. *Nat. Genet.* **54**, 705–714 (2022).
880 41. Wang, L. *et al.* A chloroplast protein atlas reveals punctate structures and spatial
881 organization of biosynthetic pathways. *Cell* **186**, 3499-3518.e14 (2023).
882 42. Kafri, M. *et al.* Systematic identification and characterization of genes in the
883 regulation and biogenesis of photosynthetic machinery. *Cell* **186**, 5638-5655.e25 (2023).
884 43. Wu, Y., Chang, L., Jiang, C., Xu, L. & Zhang, J. Plastid Transformation in Poplar: A
885 Model for Perennial Trees. in *Chloroplast Biotechnology: Methods and Protocols* (ed.
886 Maliga, P.) 257–265 (Springer US, New York, NY, 2021). doi:10.1007/978-1-0716-1472-
887 3_14.
888 44. Xu, S. *et al.* Plastid-expressed Bacillus thuringiensis (Bt) cry3Bb confers high
889 mortality to a leaf eating beetle in poplar. *Plant Cell Rep.* **39**, 317–323 (2020).
890 45. Ruf, S. *et al.* High-efficiency generation of fertile transplastomic Arabidopsis plants.
891 *Nat. Plants* **5**, 282–289 (2019).
892 46. Crozet, P. *et al.* Birth of a Photosynthetic Chassis: A MoClo Toolkit Enabling
893 Synthetic Biology in the Microalga Chlamydomonas reinhardtii. *ACS Synth. Biol.* **7**, 2074–
894 2086 (2018).

895 47. Patron, N. J. *et al.* Standards for plant synthetic biology: a common syntax for
896 exchange of DNA parts. *New Phytol.* **208**, 13–19 (2015).
897 48. Bateman, J. M. & Purton, S. Tools for chloroplast transformation in Chlamydomonas:
898 expression vectors and a new dominant selectable marker. *Mol. Gen. Genet. MGG* **263**,
899 404–410 (2000).
900 49. Cutolo, E. *et al.* A Phosphite Dehydrogenase Variant with Promiscuous Access to
901 Nicotinamide Cofactor Pools Sustains Fast Phosphite-Dependent Growth of
902 Transplastomic Chlamydomonas reinhardtii. *Plants* **9**, 473 (2020).
903 50. Sandoval-Vargas, J. M. *et al.* Use of the ptxD gene as a portable selectable marker
904 for chloroplast transformation in Chlamydomonas reinhardtii. *Mol. Biotechnol.* **61**, 461–
905 468 (2019).
906 51. Remacle, C. *et al.* The ARG9 Gene Encodes the Plastid-Resident N-Acetyl Ornithine
907 Aminotransferase in the Green Alga Chlamydomonas reinhardtii. *Eukaryot. Cell* **8**, 1460–
908 1463 (2009).
909 52. Matsuo, T., Onai, K., Okamoto, K., Minagawa, J. & Ishiura, M. Real-Time Monitoring
910 of Chloroplast Gene Expression by a Luciferase Reporter: Evidence for Nuclear
911 Regulation of Chloroplast Circadian Period. *Mol. Cell. Biol.* **26**, 863–870 (2006).
912 53. Rott, R., Liveanu, V., Drager, R. G., Stern, D. B. & Schuster, G. The sequence and
913 structure of the 3′-untranslated regions of chloroplast transcripts are important
914 determinants of mRNA accumulation and stability. *Plant Mol. Biol.* **36**, 307–314 (1998).
915 54. Eibl, C. *et al.* In vivo analysis of plastid psbA, rbcL and rpl32 UTR elements by
916 chloroplast transformation: tobacco plastid gene expression is controlled by modulation of
917 transcript levels and translation efficiency. *Plant J.* **19**, 333–345 (1999).
918 55. Tangphatsornruang, S., Birch-Machin, I., Newell, C. A. & Gray, J. C. The effect of
919 different 3′ untranslated regions on the accumulation and stability of transcripts of a gfp
920 transgene in chloroplasts of transplastomic tobacco. *Plant Mol. Biol.* **76**, 385–396 (2011).

921 56. Anthonisen, I. L., Salvador, M. L. & Klein, U. Specific sequence elements in the 5′
922 untranslated regions of rbcL and atpB gene mRNAs stabilize transcripts in the chloroplast
923 of Chlamydomonas reinhardtii. *RNA* **7**, 1024–1033 (2001).
924 57. Wilde, A. & Hihara, Y. Transcriptional and posttranscriptional regulation of
925 cyanobacterial photosynthesis. *Biochim. Biophys. Acta BBA - Bioenerg.* **1857**, 296–308
926 (2016).
927 58. Eberhard, S., Drapier, D. & Wollman, F.-A. Searching limiting steps in the expression
928 of chloroplast-encoded proteins: relations between gene copy number, transcription,
929 transcript abundance and translation rate in the chloroplast of Chlamydomonas
930 reinhardtii. *Plant J.* **31**, 149–160 (2002).
931 59. Rahim, M. M. A., Vigneault, F. & Zerges, W. The RNA Structure of cis-acting
932 Translational Elements of the Chloroplast psbC mRNA in Chlamydomonas reinhardtii.
933 *Front. Plant Sci.* **7**, (2016).
934 60. Loizeau, K. *et al.* Small RNAs reveal two target sites of the RNA-maturation factor
935 Mbb1 in the chloroplast of Chlamydomonas. *Nucleic Acids Res.* **42**, 3286–3297 (2014).
936 61. Vaistij, F. E., Goldschmidt-Clermont, M., Wostrikoff, K. & Rochaix, J.-D. Stability
937 determinants in the chloroplast psbB/T/H mRNAs of Chlamydomonas reinhardtii. *Plant J.*
938 **21**, 469–482 (2000).
939 62. Monod, C., Goldschmidt-Clermont, M. & Rochaix, J.-D. Accumulation of chloroplast
940 psbB RNA requires a nuclear factor in Chlamydomonas reinhardtii. *Mol. Gen. Genet.*
941 *MGG* **231**, 449–459 (1992).
942 63. Ossenbühl, F. & Nickelsen, J. cis- and trans-Acting Determinants for Translation of
943 psbD mRNA in Chlamydomonas reinhardtii. *Mol. Cell. Biol.* **20**, 8134–8142 (2000).
944 64. Gotsmann, V. L. *et al.* Utilizing high-resolution ribosome profiling for the global
945 investigation of gene expression in Chlamydomonas. *Plant J.* **117**, 1614–1634 (2024).
946 65. Westhoff, P. & Herrmann, R. G. Complex RNA maturation in chloroplasts. *Eur. J.*
947 *Biochem.* **171**, 551–564 (1988).

948 66. Zhou, F., Karcher, D. & Bock, R. Identification of a plastid intercistronic expression
949 element (IEE) facilitating the expression of stable translatable monocistronic mRNAs from
950 operons. *Plant J.* **52**, 961–972 (2007).
951 67. Navarrete, A. & Pollak, B. Antisense transcription from a neighboring gene interferes
952 with the expression of mNeonGreen as a functional in vivo fluorescent reporter in the
953 chloroplast of Chlamydomonas reinhardtii. 2023.11.08.566267 Preprint at
954 https://doi.org/10.1101/2023.11.08.566267 (2023).
955 68. Tao, Y. *et al.* Enhanced Photosynthetic Efficiency for Increased Carbon Assimilation
956 and Woody Biomass Production in Engineered Hybrid Poplar. *Forests* **14**, 827 (2023).
957 69. Schad, A., Rössler, S., Nagel, R., Wagner, H. & Wilhelm, C. Crossing and selection
958 of Chlamydomonas reinhardtii strains for biotechnological glycolate production. *Appl.*
959 *Microbiol. Biotechnol.* **106**, 3539–3554 (2022).
960 70. Schroda, M., Blöcker, D. & Beck, C. F. The HSP70A promoter as a tool for the
961 improved expression of transgenes in Chlamydomonas. *Plant J.* **21**, 121–131 (2000).
962 71. Schroda, M., Beck, C. F. & Vallon, O. Sequence elements within an HSP70 promoter
963 counteract transcriptional transgene silencing in Chlamydomonas. *Plant J.* **31**, 445–455
964 (2002).
965 72. Mainguet, S. E., Gronenberg, L. S., Wong, S. S. & Liao, J. C. A reverse glyoxylate
966 shunt to build a non-native route from C4 to C2 in *Escherichia coli*. *Metab. Eng.* **19**, 116–
967 127 (2013).
968 73. Hutner, S. H., Provasoli, L., Schatz, A. & Haskins, C. P. Some Approaches to the
969 Study of the Role of Metals in the Metabolism of Microorganisms. *Proc. Am. Philos. Soc.*
970 **94**, 152–170 (1950).
971 74. Engler, C. *et al.* A Golden Gate Modular Cloning Toolbox for Plants. *ACS Synth. Biol.*
972 **3**, 839–843 (2014).
973 75. Stukenberg, D. *et al.* The Marburg Collection: A Golden Gate DNA Assembly
974 Framework for Synthetic Biology Applications in Vibrio natriegens. *ACS Synth. Biol.* **10**,
975 1904–1919 (2021).

976 76. Potapov, V. *et al.* Comprehensive Profiling of Four Base Overhang Ligation Fidelity
977 by T4 DNA Ligase and Application to DNA Assembly. *ACS Synth. Biol.* **7**, 2665–2674
978 (2018).
979 77. Schada von Borzyskowski, L. *et al.* Implementation of the β-hydroxyaspartate cycle
980 increases growth performance of *Pseudomonas putida* on the PET monomer ethylene
981 glycol. *Metab. Eng.* **76**, 97–109 (2023).
982 78. Demichev, V., Messner, C. B., Vernardis, S. I., Lilley, K. S. & Ralser, M. DIA-NN:
983 Neural networks and interference correction enable deep proteome coverage in high
984 throughput. *Nat. Methods* **17**, 41–44 (2020).
985 79. Glatter, T. *et al.* Large-Scale Quantitative Assessment of Different In-Solution Protein
986 Digestion Protocols Reveals Superior Cleavage Efficiency of Tandem Lys-C/Trypsin
987 Proteolysis over Trypsin Digestion. *J. Proteome Res.* **11**, 5145–5156 (2012).
988 80. Ahrné, E., Molzahn, L., Glatter, T. & Schmidt, A. Critical assessment of proteome-
989 wide label-free absolute abundance estimation strategies. *PROTEOMICS* **13**, 2567–2578
990 (2013).
991 81. Parks, D. R., Roederer, M. & Moore, W. A. A new “Logicle” display method avoids
992 deceptive effects of logarithmic scaling for low signals and compensated data. *Cytometry*
993 *A* **69A**, 541–551 (2006).
994
995
996
997
998
999
1000
1001

Acknowledgements

We thank Vinca Seiler for creating all the illustrations of the manuscript.

Author information

These authors contributed equally: René Inckemann and Tanguy Chotel

Authors and Affiliations

René Inckemann - Max-Planck Institute for Terrestrial Microbiology, Marburg 35043, Germany; Center for Synthetic Microbiology, Philipps-Universität Marburg, Marburg 35032, Germany
Orcid: https://orcid.org/0000-0002-6221-6443;
Email: rene.inckemann@mpi-marburg.mpg.de

Tanguy Chotel - Max-Planck Institute for Terrestrial Microbiology, Marburg 35043, Germany; Center for Synthetic Microbiology, Philipps-Universität Marburg, Marburg 35032, Germany
Orcid: https://orcid.org/0000-0002-6221-6443;
Email: tanguy.chotel@mpi-marburg.mpg.de

Cedric K. Brinkmann - Max-Planck Institute for Terrestrial Microbiology, Marburg 35043 Germany; Orcid: https://orcid.org/0000-0002-3123-5385
Email: brinkmac@students.uni-marburg.de

Michael Burgis - Center for Synthetic Microbiology, Philipps-Universität Marburg, Marburg 35032, Germany; Orcid: https://orcid.org/0009-0001-4880-5372
Email: burgismi@staff.uni-marburg.de

Laura Andreas - Max-Planck Institute for Terrestrial Microbiology, Marburg 35043, Philipps-Universität Marburg, Marburg 35032, Germany;
Email: andreasl@students.uni-marburg.de

Jessica Baumann - Max-Planck Institute for Terrestrial Microbiology, Marburg 35043, Philipps-Universität Marburg, Marburg 35032, Germany;
Email: baumannu@students.uni-marburg.de

Priyati Sharma - Max-Planck Institute for Terrestrial Microbiology, Marburg 35043,
Email**:** priyati@asu.edu

Melanie Klose - Max-Planck Institute for Terrestrial Microbiology, Marburg 35043, Germany;
Email: klosem@mpi-marburg.mpg.de

James Barret - Centre for Novel Agricultural Products (CNAP), University of York**,** York YO10 5DD
Email**:** james.barrett@york.ac.uk
Fabian Ries- TU Kaiserslautern, Kaiserslautern 67663, Germany
Orcid: https://orcid.org/0000-0002-0964-3307
Email: riesf@rhrk.uni-kl.de

Nicole Paczia - Max-Planck Institute for Terrestrial Microbiology, Marburg 35043, Germany;
Orcid: https://orcid.org/0000-0003-3859-8186
Email: nicole.paczia@mpi-marburg.mpg.de

Timo Glatter - Max-Planck Institute for Terrestrial Microbiology, Marburg 35043, Germany;
Orcid: https://orcid.org/0000-0001-8716-8516
Email: timo.glatter@mpi-marburg.mpg.de

Luke Mackinder - Centre for Novel Agricultural Products (CNAP), University of York**,** York YO10 5DD ; Orcid: https://orcid.org/0000-0003-1440-3233
Email: luke.mackinder@york.ac.uk

Felix Willmund - Philipps-Universität Marburg, Marburg 35032, Germany; TU Kaiserslautern, Kaiserslautern 67663, Germany
Orcid: https://orcid.org/0000-0002-3988-4590
Email: felix.willmund@biologie.uni-marburg.de

Tobias J. Erb - Max-Planck Institute for Terrestrial Microbiology, Marburg 35043, Germany; Center for Synthetic Microbiology, Philipps-Universität Marburg, Marburg 35032, Germany
Orcid: https://orcid.org/0000-0003-3685-0894
Email: toerb@mpi-marburg.mpg.de

Contributions

R.I and T.C contributed equally. R.I. , T.C., T.J.E., and M.B. F.W, L.C.M.M. conceived, planned, and designed the study. R.I. T.C., M.B., C.K.B, L.A., J.B, P.S, J.B., M.K. , performed the experiments and data analysis. F.R. performed the western-blot experiments. J.B. performed the fluorescence microscopy and data analysis. N.P. performed the metabolomics experiments and data analysis. T.G performed the proteomics experiments and data analysis. T.J.E., R.I. T.C. , F.W. wrote and edited the manuscript with the input of all authors. T.J.E. acquired funding and supervised the work. All authors approved the final manuscript.

Corresponding authors

Tobias J. Erb
Max-Planck Institute for Terrestrial Microbiology, Marburg 35043, Germany; Center for Synthetic Microbiology, Philipps-Universität Marburg, Marburg 35032, Germany
Orcid: https://orcid.org/0000-0003-3685-0894
Email: toerb@mpi-marburg.mpg.de

Extended Data

A

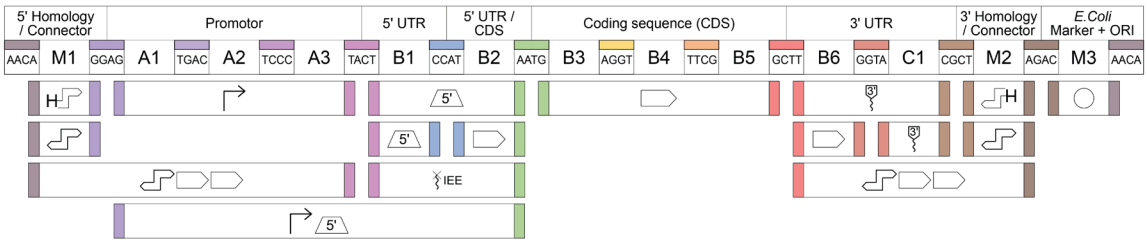

B

Types of Parts	SBOL	Part Number
Connectors		34
Homologies	H	20
Operon Connectors		14
Promoters		33
Promoters + 5' UTRs	5'	8
5' Untranslated Regions (5' UTR)	5'	53
Intercistronic Expression Elements (IEE)	IEE	17
Tags		49
Coding Sequences (CDS)		22
3' Untranslated Regions (3' UTR)	3'	43
E.Coli Markers + ORIs		8
Preassembled Vectors		21
Total		**322**

Extended Data Fig. 1: Architecture of the novel chloroplast modular cloning (MoClo) system and overview of the created genetic parts. **b,** The architecture follows the Phytobrick standard[47] and conserves the cloning overhangs of this system, as well as the nomenclature for the part types (A1-C1). The position M1-3 allow for higher modularity as reported by Stukenberg *et al.* Number of parts are indicated for each position. **b**, List of parts. Each type of parts is listed, their SBOL depicted and the number of parts associated indicated.

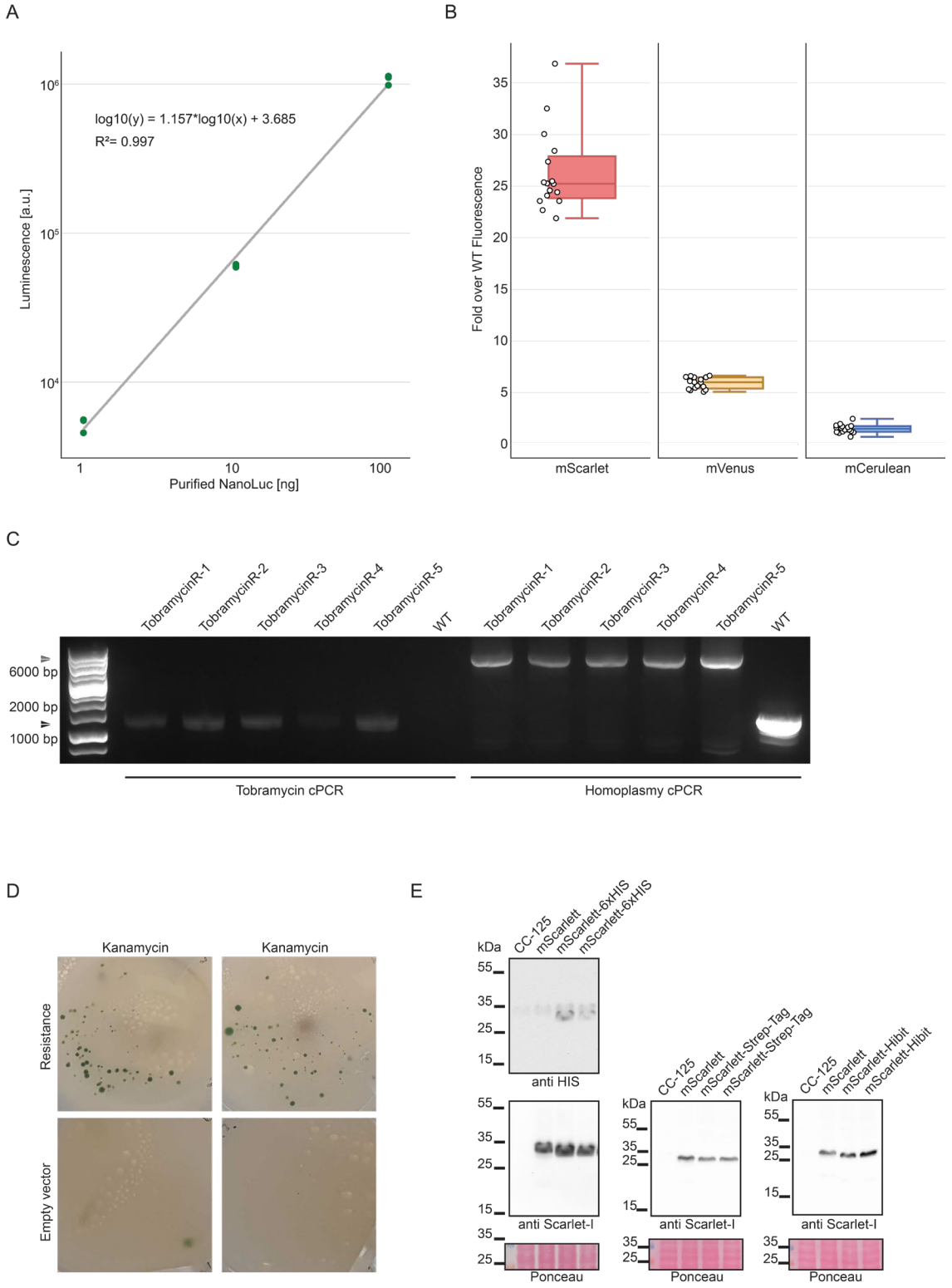

Extended Data Fig. 2: Reporters and selection markers. **a**, Calibration curve for purified NanoLuc concentration (ng) versus luminescence intensity (a.u.). The relationship between nanoluciferase abundance and luminescence is linear. **b**, Fluorescent reporter characterization. Fold over WT fluorescence is displayed for each strain, normalized by chlorophyll content, each expressing a different fluorescent reporter. $n_{biological}$=16. **c,** PCR analysis of tobramycin-resistant strains. The first section of the gel illustrates PCR products of the tobramycin resistance gene, exclusive to the five genetically modified strains, with ~1500 bp bands, absent in WT. The latter section shows PCR products from the insertion site, with ~8000 bp bands in engineered strains and a 2000 bp band in WT, indicating homoplasmy in the modified strains. **d,** Selection marker for chloroplast transformation, with two replicates and two negative controls for each one. Successful selection after chloroplast transformation can be observed. **e,** Western blot analysis of transplastomic strains producing

mScarlet HIS-tagged, Strep-tagged, Hibit-tagged in the Cterm position. Each strain is also tested for the presence of mScarlet using mScarlet specific probes. Ponceau gels are shown for each gel.

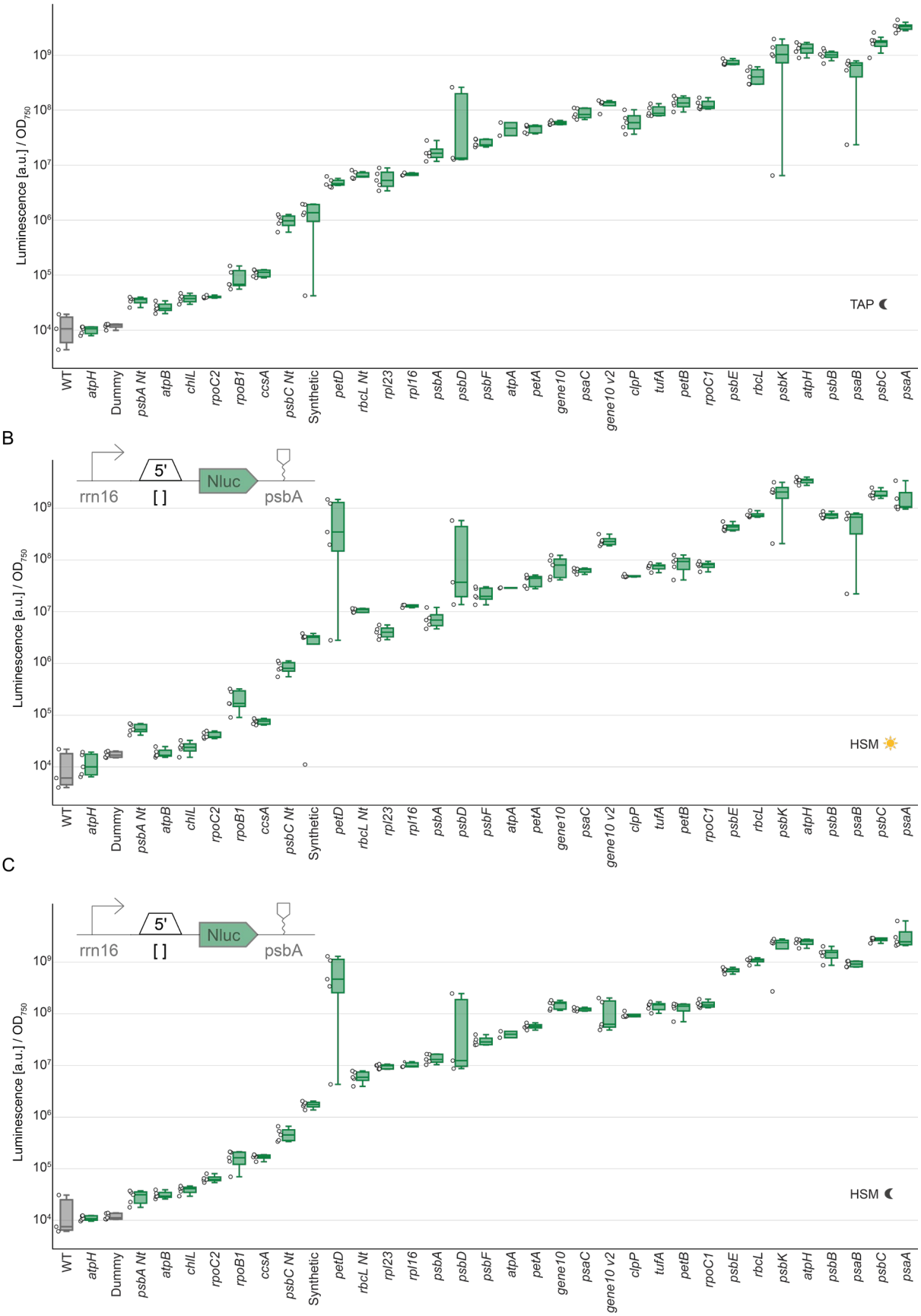

1113

1114 **Extended Data Fig. 3: Characterization of 5' UTR under different light and medium conditions.**
1115 5'UTRs were characterized by measuring NanoLuc activity of transplastomic strains containing different constructs, which
1116 differ in their 5'UTR. Nanoluc signal of a transplastomic strain containing a NanoLuc expression cassette (green) is plotted
1117 as arbitrary units [a.u.] normalized to OD and compared to WT strain (gray). For all measurements, $n_{biological}$= 5, $n_{technical}$=
1118 3. **a,** NanoLuc assay under TAP dark conditions, **b,** under HSM light conditions and **c,** under HSM dark conditions. PetD
1119 stands out under HSM conditions.

1120

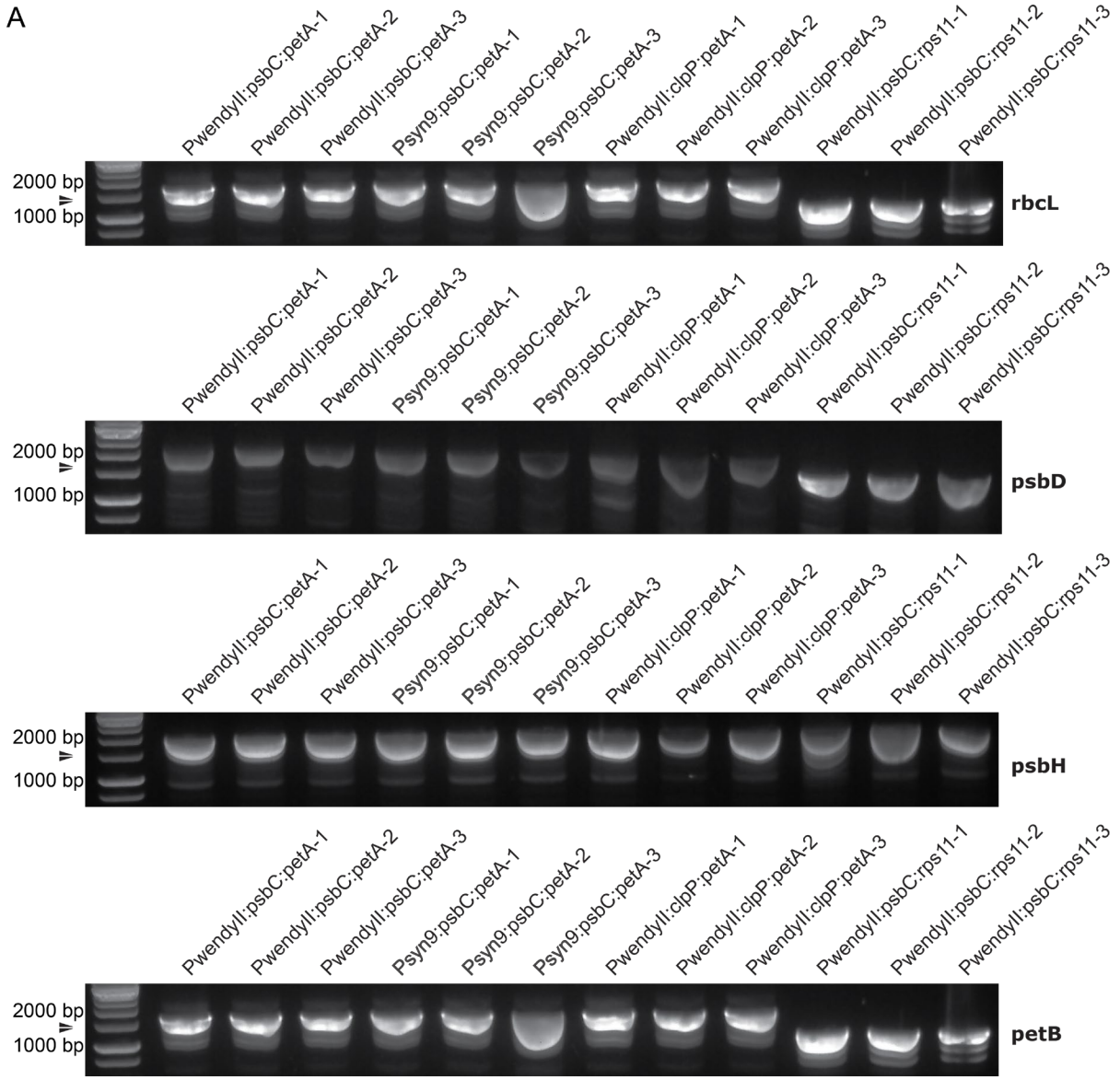

1121

1122

1123 **Extended Data Fig. 4: Genotyping of transplastomic strains.** Gel depiction of cPCR amplification for the NanoLuc
1124 reporter gene across transplastomic strains shown in Figure 5c, with four distinct constructs integrated at separate sites
1125 in the genome. For each construct, $n_{biological}$=3. A unique band, ranging from ~1500-2000 bp, is visible in genetically
1126 modified strains across all four constructs and integration sites, but is not present in the WT.

1127

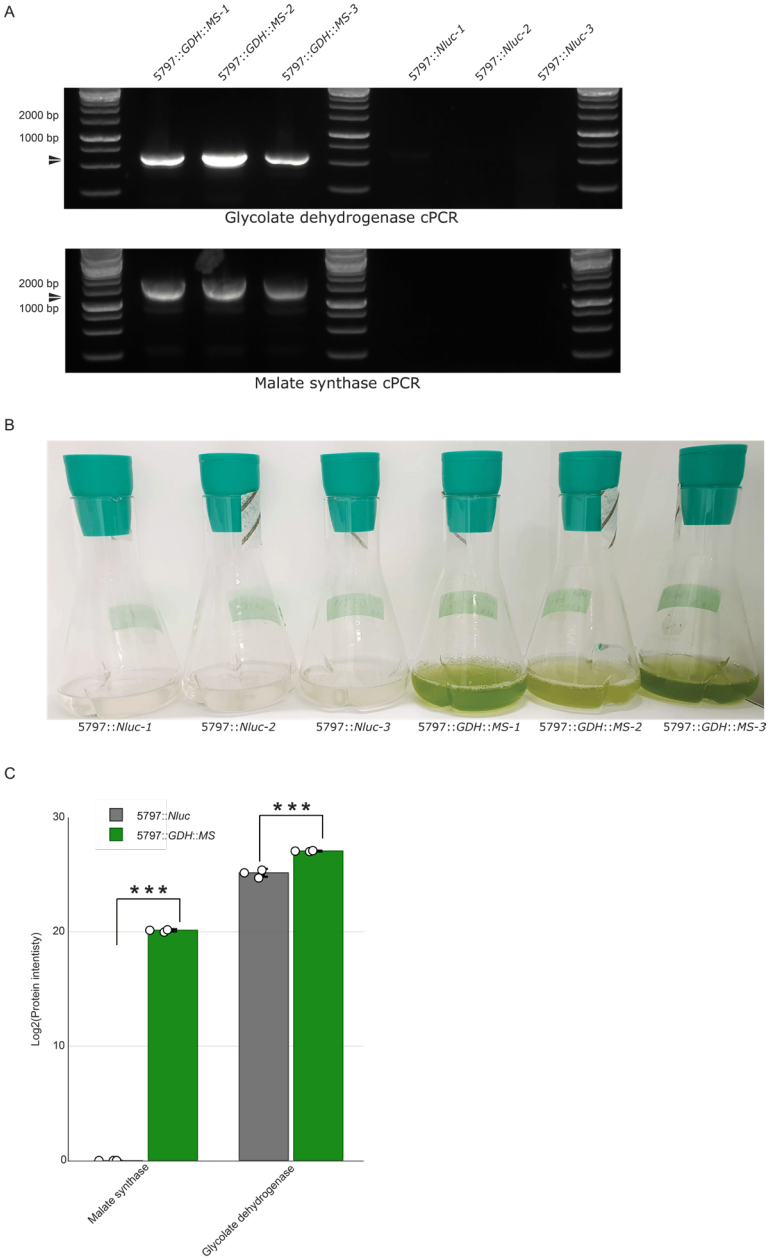

Extended Data Fig. 5: Genotyping and phenotyping of transplastomic strains containing the synthetic photorespiratory bypass. a, Gel depiction of cPCR amplification for the two heterologous genes glycolate dehydrogenase (GDH) and Malate synthase (MS) gene across transplastomic strains shown in Figure 6c-k. A unique band of ~500 bp and 1500bp, for GDH and MS respectively, is visible in genetically modified strains but is not present in the control (5797::Nluc). For each experiment, $n_{biological}$=3. **b,** Phenotypic comparison of strains expressing GDH and MS after 15 days. The image presents three biological replicates of the 5797::*GDH*::*MS* strain, demonstrating robust and dense growth. In contrast, control strains (5797::*Nluc*) exhibit no further growth. **c**. Proteomic analysis of the modified strains. The chart compares protein levels of MS and GDH in both the 5797::*GDH*::*MS* and 5797::*Nluc* strains, revealing significantly higher protein intensities in the 5797::*GDH*::*MS* strain for both proteins. Statistical significance is denoted by *** for a p-value < 0.001 (MS p-value < 0.000001, GDH p-value = 0.000623).